UNIVERSITY OF CALIFORNIA

Santa Barbara

Estuarine Response to Disturbance: A Holocene Record of Storm Episodes and Seismicity as Preserved in Coastal Systems

A Thesis submitted in partial satisfaction of the

requirements for the degree Master of Science

in Earth Science

by

Dillon J. Osleger

Committee in charge:

Professor Alex Simms, Chair

Professor Edward A. Keller

Professor Oliver Chadwick

June 2018

The thesis of Dillon James Osleger is approved.

_____

Edward A. Keller

_____

Oliver Chadwick

_____

Alex Simms, Committee Chair

May 2018

Estuarine Response to Disturbance: A Holocene Record of Storm Episodes and Seismicity as Preserved in Coastal Systems

ACKNOWLEDGEMENTS

The author thanks the Santa Barbara Long Term Ecological Research center, the Geological Society of America, and the Southern California Earthquake Center for funding this work including drilling, analyses and GSR Support. Additionally, thanks are owed to Dr. John Southon for radiocarbon dating, Dr. Ana Ejarque for XRF analysis, and the UC Davis Stable Isotope Facility for isotope analysis. Field assistance from Dr. Elizabeth Steel, Daniel Livsey, Zack Nelson, Angela Roman, Laura Reynolds, and John Munson are greatly appreciated.

ABSTRACT

Estuarine Response to Disturbance: A Holocene Record of Storm Episodes and Seismicity as Preserved in Coastal Systems

by

Dillon James Osleger

Southern California is highly susceptible to hazards related to seismic activity and storms linked with El Niños and Atmospheric Rivers. These hazards are capable of incurring flooding, debris flow, coastal inundation, and rapid coastal erosion. Although much work has been done using lacustrine and deep marine sediment records to reconstruct the frequency of these past events, coastal records from lagoons and estuaries are less well documented. Here we present detailed sedimentologic and geochemical analysis of sediment cores, constrained by radiocarbon dates, from two estuarine/lagoon systems from coastal Southern California, Campus Lagoon and Las Salinas Lagoon. Our results record multiple occurrences of marine inundation thought to record storms of similar or greater magnitude as the catastrophic winter storms of 1861-1862. At least three of these events occurred pre 149 calibrated years before present (CYBP), one between 149 and 397 ± 22, two between 397 ± 22 and 617 ± 105 CYBP, and three between 1050 ± 200 and 3400 ±190 CYBP. These events establish a historic recurrence interval of ~660 years, and a post 2000 CYBP interval of 320 years, comparable to other California records. However, two of these pre-1 ka events may be the result of tsunami washover rather than storm washover as they correlate to large magnitude seismic earthquakes along the Pitas Point fault at 1050 ± 200 and 2250 ± 300 CYBP. A simultaneous environmental shift from an open lagoon to barrier-lagoon is observed in both lagoons at 4300 ± 250 CYBP that is interpreted

to represent the onset of beach progradation in the Santa Barbara Channel in response to slowing sea-level rise.

Table of Contents

1) Introduction

Predictions of future climate change in a warming environment suggest greater climate variability and amplitude (Noren et al., 2002; Kennett et al., 2007; Shields and Kiehl, 2016). This shift in climate variability may be expressed by an increase in severity of catastrophic events, including droughts and high-intensity storms (Neiman et al., 2013; Dettinger, 2011). Assessment of future climate variability within this region is dependent on a baseline of past events under varying climates. Existing records of past droughts and severe storms have been constructed on a range of time scales, including historical records (Engstrom, 1996), marine sediment cores (Hendy et al., 2013), dendrochronology (Hurteau et al., 2007), and lacustrine records (Bird and Kirby, 2006; de Jong et al., 2006; Osleger et al., 2009; Dingemans et al., 2014; Kirby et al., 2010). Southern California are also potentially susceptible to tsunamis (Borrero et al., 2004; Ryan et al., 2015) associated with large ($M_w > 7$) earthquakes, which may leave a sedimentologic signature comparable to that of storm washover (Morton et al., 2007). These archives provide a look at the impact of such severe storms and seismic events on the broader region, but few datasets exist regarding how these hazards impacted the most heavily populated parts of southern California – its coastline (Ejarque et al., 2015; Kirby et al., 2007; Reynolds, 2018).

Campus Lagoon on the University of California Santa Barbara (UCSB) campus and Las Salinas Lagoon (now the Andree Clark Bird Refuge) in the city of Santa Barbara are investigated in this study in order to better determine the frequency of past catastrophic events including severe storms and tsunamis. The objective of this

investigation is to determine environmental changes recorded within lagoon systems along the Santa Barbara coastline through the mid- to late Holocene. Two specific research questions are addressed regarding hazards that impacted this system over the Holocene: A) What is the frequency of severe storm events recorded within the sedimentological record? B) Is evidence for tsunamis found within these systems?

1.1) Regional Setting

Campus and Las Salinas lagoons are located along the east-west trending mesotidal coastline of the Santa Barbara Channel of Southern California in the city of Santa Barbara (Figure 1). The region lies within the Santa Barbara Fold and Thrust Belt (SBFTB), which is a series of east-west trending folds and faults resulting from contraction in response to the geometry of the San Andreas Fault (Keller and Gurrola, 2000; Keller and DeVecchio, 2013). Marine terraces surrounding the study sites are indicative of high uplift rates along one or more of the structures underlying the Santa Barbara area (Gurrola et al., 2014).

The study area lies within the Santa Barbara Littoral Cell, one of the five major littoral cells of the Southern California Bight (Inman et al., 2005). Littoral cells, natural compartments that occur on all coasts, contain the sources, transport paths, and sinks of sediment (e.g. Inman et al., 2005 Masters, 2006). Sediment is brought into the Santa Barbara littoral cell by streams and rivers with sea cliffs providing a minor contribution (Patch and Griggs, 2006). This sediment flux is dependent on precipitation and streamflow, with its redistribution reliant on prevailing wave direction and longshore currents.

Campus Lagoon

Currently, Campus Lagoon is largely isolated from terrestrial input with no connection to any sizable stream. Its dendritic shape may be a reflection of a more substantial former stream network sourced from a larger drainage basin during the Quaternary subsequently removed by bluff erosion or cutoff by uplift along the More Ranch Fault. Prior to modification, its mouth opened to the ocean, which may have been blocked at times by the buildup of a bay-mouth bar as seen in T-sheets from 1852 (San Francisco Estuary Institute). The lagoon lies to the south and within the hanging wall or upthrown side of the More Ranch Fault (Figure 2) and to the north of the north-dipping Red Mountain and Pitas Point faults (Figure 1).

Las Salinas Lagoon

Prior to modification, Las Salinas Lagoon was fed from the north by Sycamore Creek (Tsheet: San Francisco Estuary Institute), providing a terrestrial connection with the Santa Ynez Mountains. Prior to anthropogenic modification, this creek likely drove canyon incision during the Last Glacial Maximum. The river valley backfilled to form Las Salinas Lagoon as RSL rose during the Holocene similar to other last glacial maximum incised valleys (Masters and Flemming, 1983). Las Salinas Lagoon is located in a subsiding synclinal basin bound to the west by the Mesa Fault to the east by the Santa Barbara Cemetery Fault and to the north by the Mission Ridge Fault (Figure 3) (Dibblee, 1966; Gurrola et al., 2014). Las Salinas Lagoon is also located to the north of the north-dipping Red Mountain and Pitas Point Faults (Figure 1).

2) Background

2.1) Atmospheric Rivers

Atmospheric Rivers (AR) are concentrated zones of horizontal water vapor transported across mid-latitude regions (Zhu and Newell, 1998) commonly resulting in orographic precipitation that triggers premature snowmelt, river flooding, and landslides (Dettinger et al., 2011). Along coastlines, ARs commonly produce strong winds and low-pressure conditions (Ralph et al., 2006; Waliser and Guan, 2017) conducive to high surf and coastal inundation. Reynolds et al. (2018) have shown that a series of AR storms that struck the California coast in the winter of 1861-1862 resulted in not only inland river flooding throughout Southern California (Engstrom, 1996), but also significant coastal inundation and overwash within Carpinteria Slough, a southern California marsh. Overwash from the 1861-1862 storm left a sand bed up to 50 cm thick extending over 450 m inland from the coastline (Reynolds et al., 2018). However, the depositional conditions at Carpinteria Slough do not allow for the recording of older storms and little is known about the frequency of coastal inundation by such events.

Weather patterns in the coastal Southwest United States, specifically high volume precipitation events like AR storms, are driven by sea surface temperatures (SST) of the Pacific Ocean and atmospheric circulation (Pyke and Bedell, 1972; Trenberth and Hurrell, 1994; Namias et al., 1988). The frequency of storms in the coastal Southwest US, including AR storms, are more frequent during periods of colder than average SST in the Northeast Pacific, which drive a southerly depression in the polar jet stream (Namias et al., 1988; Fye et al., 2009; Cook et al., 2011; Kirby et al., 2012). El-Niño-Southern Oscillation (ENSO) and the Pacific Decadal Oscillation (PDO),

which play major roles in driving SST fluctuations and thus the amount of winter precipitation received across the coastal Southwest US (Cayan et al., 1999), may play a role in governing AR storms. These processes are known to drive higher winter precipitation in the coastal Southwest US during El Niño events and positive PDO cycles; however, their relationship with the frequency of AR storms is poorly understood (Dettinger, 2011; Cook et al., 2011).

2.2) Regional Seismicity

Recent work by Rockwell et al. (2016) in the SBFTB has identified four Holocene uplifted marine terraces thought to have resulted from co-seismic uplift near Pitas Point east of the study area (Figure 1). These events triggered 7 to 12 meters of discrete uplift, which, based on similar studies comparing discrete uplift to magnitude (Rubin et al., 2001), have been argued to represent magnitude 7 or 8 earthquakes (Rockwell et al., 2016). Their frequency implies that the western Transverse Ranges and the Santa Barbara Basin may experience large magnitude ($M_w > 7$) earthquakes every ~900 yr in response to ruptures on the Pitas Point and Lower Red Mountain faults within the SBFTB (Rockwell et al., 2016). Numerical models suggest that these earthquakes have the potential of producing tsunami with heights of 6-8 m (Ryan et al., 2015).

Uplifted marine terraces on the UCSB campus include a 48,000 year-old marine terrace at a modern elevation of 14 m and an undated Holocene marine terrace at ~1 m of elevation (Gurrola et al., 2014). These marine terraces, as well as others across the northern Santa Barbara Channel (Upson, 1951) attest to high rates of uplift along

one or more structures within the SBFTB (Gurrola et al., 2014; Minor et al., 2009). Possible structures responsible for uplift across the study area include the North Channel-Pitas Point fault system (NPF) and the Red Mountain fault (RMF) (Johnson et al., 2017) (Figure 1). The More Ranch Fault may also contribute to uplift of the area around Campus Lagoon (Gurrola et al., 2014).

Two estimates have been determined for uplift rates of the 48 ka marine terrace: 1.6 mm/yr based on a comparison between the marine terrace height and regional late Pleistocene sea levels (Gurrola et al., 2014), and 0.15 mm/yr based on a comparison between the elevation of a *Cerithidea californica*, an intertidal gastropod, and a regional Holocene sea-level reconstruction (Simms et al., 2016). The lack of a mid-Holocene highstand along the Southern California coast (Reynolds and Simms, 2015) suggests the lower Holocene terrace records uplift continuing into recent times. However, the elevations and long-term uplift rates of these terraces cannot be used to differentiate whether uplift is gradual or results from punctuated episodes of abrupt uplift during earthquakes.

3) Methodology

3.1) Core acquisition

Nine 7.6-cm diameter vibracores ranging from 0.5 m to 4 m in length were collected in Campus and Las Salinas lagoons. Two cores were taken from the Andree Clark Bird Refuge within Las Salinas Lagoon (Figure 3) and seven cores were taken aboard a floating drilling platform from Campus Lagoon on the UCSB campus

(Figure 2). Cores were split (with half archived), photographed, described, and sampled within the Sedimentology Laboratory at the University of California Santa Barbara.

3.2) Textural and Mineralogical analysis

Cores were described following the methods of Boyles et al. (1986) in order to standardize the description of sedimentary units. This method provides guidelines for the non-interpretive descriptions of grain size, boundary transitions, color, biologic inclusions within sediments, and stratigraphy within a section of either consolidated or unconsolidated sedimentary material. Mineralogy was determined by repeated point counts of quartz, feldspar, and lithic fragments within 0.5 cm^3 samples. Point count values were averaged from sets of 5 counts, with each set consisting of 200 identified grains in the microscope (10x) oculus of a given sample.

Grain-size analysis was conducted on five cores at 2.5-cm intervals through mud/clay deposits and 1-cm intervals through sand deposits. 0.5 cm^3 of sediments from the cores were mixed with 100 ml of 5.5 g/L sodium metahexaphosphate to prevent flocculation of clay particles following pretreatment with 30% H_2O_2 and 1 N HCl at 200^oC to 270^oC to remove carbonates and organics respectively. The pretreated suspended sediments were analyzed using a CILAS1190L particle-size analyzer following the methods of Sperazza et al. (2004) to quantitatively determine changes in grain size and grading throughout the core.

3.3) Radiometric Dating and Age Model

Forty-two charcoal and carbonate samples, including samples taken to bracket sharp contacts and large depositional events, were removed for ^{14}C dating analysis. Radiocarbon material removal and dating was conducted following the methods prescribed by the W.M. Keck Carbon Cycle Accelerator Mass Spectrometry (AMS) Laboratory at the University of California Irvine (Olsson and Berglund, 1986).

All dates were corrected to calibrated years before present (CYBP) using the online CALIB program version 7.1.0 in association with the intcal09.14c calibration data set (Reimer et al., 2013; Stuiver and Reimer, 1993) for in text dates and within the R-model Bchron (Haslett and Parnell, 2008) for ages used within age models. All charcoal radiocarbon dates were calibrated using the North American Atmospheric curve while carbonate ages were calibrated using the Northern Hemisphere Marine Reservoir with a local reservoir correction of 217 ^{14}C years made against the global marine carbon reservoir of 440 years (ΔR; Stuiver et al., 1998) for all carbonate ages due to the influence of fluvial derived organic material in Southern California estuaries (Holmquist et al., 2015).

The statistical Bayesian probability model Bchron (Haslett and Parnell, 2008) was used to model age uncertainties. This method accounts for outliers and interruptions (Parnell et al., 2011). For a comprehensive review on the approaches and benefits of this program see Scholz et al. (2012).

3.4) XRF and CIA

X-Ray Fluorescence analysis was conducted on core AC15-01 from Las Salinas Lagoon. XRF scans were carried out on 20 cm long mini core sections, cataloguing

elemental composition every 0.5 cm at the French National Centre for Scientific Research by Dr. Ana Ejarque with data provided in corrected weight percent format. The suite of data reported in text and figures includes aluminum, sulfur, calcium and strontium while additional elements measured can be found in supporting material. Elemental data were converted to PPM, normalized to Mole %, and translated to chemical index of alteration (CIA) using models originally defined in Nesbitt and Young (1982) in order to quantify degrees of silicate weathering. CIA was calculated via

$$CIA = Al_2O_3 / (Al_2O_3 + CaO + Na_2O + MgO)*100) \quad (1)$$

to account for burial metasomatism ($^{K+}$ uptake by clay). CIA has been shown to function as a geochemical proxy for mean annual precipitation (Sheldon et al., 2002; Gulbranson et al., 2011). This proxy has not yet been used within estuarine or lagoon systems, which collect material as a result of weathering, but has been successful on a wide temporal range, including paleosols and modern soils (Gulbranson et al., 2011), as well as runoff from major rivers in China (Li and Yang, 2010). As few studies have used CIA within estuarine environments, we present results from modeling as units of weight to mole percent (CIA eq. 1) instead of mm of precipitation, resulting in a relative scale of weathering. Here we employ this proxy in a novel setting, observing trends with respect to facies to test the hypothesis that deposits interpreted to represent intense weathering should coincide with peaks observed in CIA results.

3.5) Carbon and Nitrogen analysis

Geochemical analyses of bulk organic fraction were performed on four cores from the two coastal systems. These analyses were carried out at a 6-cm sample spacing, with a higher sampling interval of ~2 cm at intervals near facies contacts. Intervals displaying correlative trends between geochemical and physical data were sampled at a finer spacing (~1 cm) in order to better constrain trends. The analysis of total organic carbon (TOC) and total nitrogen (TN) was performed through the treatment of samples with 1 N HCL for 24 hours to remove carbonates and neutralize residues with ultrapure water. Isotopic ratios, $\delta^{13}C_{org}$ and $\delta^{15}N$ yields (micrograms) were analyzed via Carlo Erba elemental analyzer connected to a Europa Scientific isotope ratio mass spectrometer at the Department of Plant Sciences, University of California, Davis. C and N yields allowed for the calculation of weight percent C and total N within the sample. Results are presented as weight percent C (%C) and C to N ratios (C/N) as these metrics are better suited to interpret source material.

External precision for samples, calculated from repeated analysis of a sucrose standard (n= 12 $\delta^{13}C_{org}$ of -21.69‰) is better than 0.06‰ for $\delta^{13}C_{org}$ and better than 1% and 1.5% for C and N content, respectively.

3.6) Subsidence and uplift estimation

Subsidence and uplift calculations followed the methods outlined in Simms et al. (2016). Magnitudes of subsidence and uplift (S) were calculated by subtracting paleo-relative sea-level elevations derived from *C. californica* shells in estuarine cores (RSL_{cc}) from the regional tectonically-corrected relative sea-level curve (RSL_{p}) of Reynolds and Simms (2015).

$$S = RSL_p - RSL_{cc} \quad (2)$$

NOAA tide gauge 9411340 was used to determine the difference between NAVD88 sea level measured by the GPS and local mean sea level. This offset was applied to the elevation of *C. californica* samples found in cores from Las Salinas and Campus Lagoons to determine their relationship to past local mean sea level.

Past relative sea level represented by the elevation of *C. californica* in cores (RSL_{cc}) was calculated by subtracting the indicative meaning of *C. californica* (IR_{cc}) from the elevation of *C. californica* specimens in cores (El_{cc}). Indicative meaning is measured as the vertical distance between a datable sedimentary horizon and its local, contemporary MSL (Zong and Sawai, 2015). Based on the work of (Sousa, 1983), *C. californica* is thought to have an indicative meaning of 0.8 ± 0.45 m.

$$RSL_{cc} = El_{cc} - IR_{cc} \quad (3)$$

The combined error (E_t) for the total magnitude of Holocene subsidence was calculated using the equation:

$$E_t = (E_{rsl}^2 + E_{obs}^2)^{0.5} \quad (4)$$

where E_{rsl} is the error assigned to the regional relative sea-level curve and E_{obs} is the vertical error associated with the RSL_{cc} of each system. Error of Holocene-averaged subsidence rates (E_r) was calculated by:

$$E_r = (S/T_{cc}) * ((E_{Tcc}/T_{cc})^2 + (E_t/S)^2)^{0.5} \quad (5)$$

where T_{cc} is the age of C. *californica* and E_{Tcc} is the error in that age.

4) Results

4.2) Sedimentological Analysis

4.2.1.) Sedimentary Facies

Six sedimentary facies were identified within the cores studied (Figure 4). These include: a muddy silt facies, a modern variant of the muddy silt facies, two distinct sand facies, a shell hash facies, and an evaporite facies.

Muddy Silt Facies

The most common facies observed in cores from both Las Salinas and Campus Lagoons is a muddy silt facies (MSF), a mottled grey to dark brown (10YR 3/2) clay-rich silt with minor amounts (<10%) of shell and organic material (Figure 4A). Roots and charcoal are found throughout this facies, with modern roots dominating the upper 5cm when the facies is found at the top of cores sampled. Beds of this facies range in overall thickness from 10 cm to 140 cm. In both systems this facies contains a transition from articulated specimens of *Cardiidae* bivalves found at its base to intact *Cerithidea californica,* an intertidal gastropod, found farther up section. Foraminifera communities within this facies are typically composed of *Elphidium* spp. and agglutinated forms. This facies commonly occurs within the upper beds of cores extracted from (pre-artificial development) areas within the lagoon environments. Beds of this facies show enrichment in $\delta^{13}C_{org}$.

Modern Muddy Silt Facies

A variant of the muddy silt facies was found at the top of cores from both Campus and Las Salinas Lagoons, consisting of similar sedimentary characteristics, but containing modern roots and more organic material than the muddy silt facies. Radiocarbon dates from within this facies calibrate to post atmospheric nuclear weapons testing, indicating their deposition sometime after 1950.

Sand Facies 1

Sand facies 1 (SF1) is composed of a moderately-sorted, bioturbated, grey (10YR 5/1) sand (>80%) with little to no clay (Figure 4B). The average D50 for this unit is 200 μm while the average D90 is 430 μm. The mineralogical composition of the sands within this facies is dominantly quartz (80%) with lithic and feldspar grains each composing on average 10% of the grains (Figure 5). Little plant material is found within beds of this facies; however, articulated bivalve shells of the species *Tresus nuttalli* are common (1-2 per 20 cm of bed).

Sand Facies 2

Sand facies 2 (SF2) is dominantly composed of 10YR 7/2, well-sorted sand (>75%) with sparse interspersed thin laminae of silt (Figure 4C&D). Grain-size within beds of this facies average 200 μm (D50) with a D90 of 390 μm. Mineralogical composition of this facies is dominated by quartz (80%) with lithic and feldspar grains comprising 15% and 5% of the sand grains, respectively (Figure 5). Marine plant fragments and occasionally shell fragments are observed within this

facies (<5%). Beds (3 in Las Salinas Lagoon and 4 in Campus Lagoon) of this facies are found interbedded with facies MSF.

Shell Hash Facies

The shell hash facies (SHF) is composed of shell fragments (>60% volume) and fecal pellets in a matrix of clayey silt (Figure 4F). Shell fragments within this facies are too small and fragmented to identify; however, fecal pellets resemble those of intertidal worms prolific in distressed environmental conditions (Shin et al., 2014). This facies is only found within core CL16-01 (Figure 6) obtained from the western, most inland, portion of Campus Lagoon. The single 22-cm thick bed of this facies is found at a depth of 200 cm within core CL16-01 in Campus Lagoon.

Evaporite Facies

The evaporite facies (EF) is composed of abundant (>60%) gypsum crystals (~250 μm) in a matrix of clayey silt (Figure 4E). This facies is only found within cores CL16-1 and CL14-01 obtained from the most-inland portions of Campus Lagoon. This facies contains little organic material, lacking plant organic matter, foraminifera, bivalves, gastropods, and bioturbation.

4.2.2) Chronology

Twenty-five radiocarbon ages were obtained from cores in Campus Lagoon (Figure 6) and 17 additional ages were obtained from cores from Las Salinas Lagoon (Figure 7). The oldest ages in stratigraphic order, 4871 ± 61 CYBP (CL16-01) and

4425 ± 41 CYBP (AC15-01), from Campus Lagoon and Las Salinas Lagoon respectively, suggest our record spans the last 4.3-4.8 ka.

The youngest beds of SF2 within Campus Lagoon are found within cores CL13-02 and CL16-03/04 at a depth of 35 to 55 cm with above and within age brackets between 149 ± 48 and 393 ± 22 (Table 2). Another bed of SF2 is found immediately below this group at a depth of 105 cm in CL13-02 and 50cm in CL16-03/04 with age brackets between 393 ± 22 and 534 ± 76. These beds of SF2 are found in single amalgamated packages at a depth of 38 cm in CL14-01, with an age bracketed to between 388 ± 41 CYBP 3 cm above its upper contact (35 cm CL14-01) and 607 ± 35 CYBP a cm below its lower contact (60 cm CL14-01). CL13-01 contains a bed of SF2 at a depth of 35 cm in a similar age bracket of 257 ± 30 within and 617 ± 105 two cm below its lower contact. Core CL13-01 displays two closely spaced beds of SF2 between 90 cm and 150 cm, which correlate to an amalgamated bed of SF2 at 200 cm in CL16-02. These paired beds of SF2 are bracketed by ages of 2581 ± 47 (110cm CL16-02) and 4425 ± 108 CYBP (250 cm CL16-02), providing a Bchron estimated age of 3400 ± 150.

The transition from MSF to SF1 within the middle lagoon is marked 10 cm above the contact by a radiocarbon age of 4425 ± 108 CYBP (CL16-02 250CM). This is concurrent with the transition from SHF to SF1 in the back lagoon marked by a radiocarbon date from within the bed of SHF (238 cm CL16-01) yielding an age 4473 ± 63 CYBP. The bed of SHF is further constrained by an age of 4871 ± 61 CYBP 23 cm below its lower contact (250 cm CL16-01) and an age of 3257±200 CYBP 38 cm above its upper contact.

Cores AC15-01 and AC15-02 from Las Salinas Lagoon each contain 3 beds of SF2. These beds are found at depths of 75 cm, 180 cm, and 240 cm in core AC15-01 and depths of 50 cm, 130 cm, and 210 cm in core AC15-02 (Figs 6 and 8). While the chronology associated with these cores appears un-correlated when viewed in cross section, Bchron age depth models utilizing methods from Wright et al. (2017) demonstrate these cores correlate both sedimentologically and chronologically to within reasonable error. Bchron age models from both cores provide estimated ages of beds at 1050 ± 200 and 2250 ± 300 CYBP and 3400 ± 200 CYBP respectively (Supplementary Figure 4). The transition of MSF to SF1 within Las Salinas Lagoon is marked by a radiocarbon age of 3597 ± 170 CYBP 5 cm above the transition (AC15-01 340 cm).

4.2.3) Campus Lagoon Stratigraphic Architecture

All cores from Campus Lagoon contain a 20-40 cm thick bed of modern MSF facies containing plant debris at their tops. However, beneath that bed, cores from the back of the lagoon (CL14-01; CL16-01), the central portions of the lagoon (CL16-02; CL13-02), and the lagoon mouth (CL13-01; CL16-03; CL16-04) each contain a different succession of facies (Figure 6).

At the base of core CL16-01 from the back of the lagoon is a 90 cm thick unit of bioturbated SF1 that appears to extend into the central lagoon. Above this sand in CL16-01 is a 22 cm thick bed of the Shell Hash Facies with a high concentration of fecal pellets (Figure 6). This is the only occurrence of this facies in both lagoons. Above the Shell Hash Facies in core CL16-01, a 160 cm thick unit of the Evaporite

Facies (EF) is found. A similar Evaporite facies bed is found above SF1 in the other core (CL14-01) from the back lagoon. The facies of EF and SF1 in CL16-01 exhibit a fining-upward succession (Figure 8).

The two cores from the central lagoon (CL16-02 & CL13-02) contain a bed of SF1 at their base that likely correlates with the SF1 bed at the base of CL16-01 in the back of the lagoon (Figure 6). A thin bed of MSF containing articulated bivalves in both cores coarsens upward transitioning sharply into a bed of SF2. Overall, no fewer than 3 beds of SF2 are found within the central lagoon. In core CL13-02, an upper bed of SF2 is found at a depth of 20 cm with two additional beds found between 148 and 183 cm. The upper bed of SF2 pinches out before core CL16-02 while the two lower beds appear to be amalgamated within core CL16-02. The interbedded MSF and SF2 beds appear to be the lateral equivalent of the evaporite facies found within cores from the back of the lagoon. The bed of SF2 within CL13-02 (100-150 cm) contains an internal amalgamation surface.

The three cores (CL13-01, CL16-03, CL16-04) obtained from the lagoon mouth (Figure 6) are composed of no fewer than 9 beds, some separated by internal amalgamation surfaces and beds of MSF interbedded with SF2. At least one of these beds appears to continue landward and correlate with the upper bed of SF2 in core CL13-02 from the central lagoon. The basal sand (SF1) bed in the back and central portions of the lagoon is absent in cores from the lagoon mouth. This unit may be present beneath the cores in this section; however, our cores failed to penetrate through the thicker upper beds of facies SF2 and MSF.

4.2.4) Las Salinas Lagoon Stratigraphic Architecture

The basal bed(s) of SF1 widespread in cores from Campus Lagoon also occurs at the base of both cores from Las Salinas Lagoon (Figure 7). SF1 in LSL is similar not only in sedimentologic characteristics as those beds in Campus Lagoon but also in age. Beds of SF2 are thicker in core AC15-02 from the more seaward portion of the lagoon compared to those of core AC15-01 from the interior of the lagoon (Figure 7). In core AC15-01, the upper three sand beds at 90 cm, 195 cm, and 260 cm have similar D50 grain size and mineralogical composition; however, the bed at 195 cm exhibits normal grading. The thicker sands of SF2 in core AC15-02 are massive and uniform, distinct from adjacent units of the Muddy Silt Facies. Beds of SF2 in core AC15-01 coincide with decreasing levels of metals (Al, Ti, Fe). The bed of SF2 at 260 cm exhibits a distinct increase (10x) in sulfur not observed in the other beds of SF2 (Figure 9). Overall, facies observed in Las Salinas Lagoon are similar to those described in Campus Lagoon, with the exception of SF2. Beds of SF2 described in Las Salinas Lagoon contain woody terrestrial plant material not observed in CL as well as silt and lithic fragments comprising a greater percentage of their composition (Figure 5. QFL in LSL 78, 13, 9. Vs QFL in CL 81, 10, 9.).

4.3) XRF analysis

The elements Al, S, Ca, and Sr are commonly used as proxies for interpreting a marine versus terrestrial source of a deposited material. XRF results from core AC15-01 are simplified to show these four elements of interest (Al, S, Ca, Sr) (Figure 9).

Beds of sand facies 2 at depths of 100 cm, 160 cm, and 260 cm show peaks in Ca and Sr concentration. A single bed of the muddy silt facies (MSF) at a depth of 20 cm displays similar peaks in Ca and Sr concentration to those observed in sand facies 2. This peak in a bed of MSF is found within the anthropogenically disturbed upper 30 cm of the core. A single peak in sulfur is found at 260 cm at the bottom contact of the lowest bed of SF2. Aluminum drops below average/peak concentrations coinciding with SF2 beds; however, shifts of this cation are less pronounced than shifts in other cations, suggesting terrestrial input may only play a minor role in the deposition of material within Las Salinas Lagoon compared to marine processes.

4.4) CIA analysis

As described in the methods section, CIA results presented here are given as a CIA ratio rather than as precipitation in mm because of the uncertainty in using a terrestrially-derived conversion to estuarine sediments. Thus, CIA is interpreted on a relative scale and interpreted as a proxy for the influx of weathered material rather than precipitation. The CIA model for Las Salinas Lagoon core AC15-01 displays peaks at 80 cm and 190 cm as well as a shift to higher values at 330 cm. The two peaks observed at 80 cm and 190 cm are both larger in magnitude (13 ± 4.5) than the average CIA trend over time; however, the latter of these two has longer and higher rising and falling limbs. Both of these peaks correspond with beds of SF2, yet a CIA peak does not mark the third bed of SF2. The shift at 330 cm has a value of 25, ~2x the magnitude of those observed at 80 cm and 190 cm and corresponds to the

transition into facies SF1. The elevated CIA values starting at 330 cm continue throughout the rest of core AC15-01.

4.5) Carbon and Nitrogen Analysis

In 3 cores from Campus Lagoon (CL16-01, CL16-02, & CL13-01), weight percent Carbon (%C) ranges from <1 wt% to 5.7 wt% (Figure 10). %C commonly exhibits abrupt shifts to lower values within most cm-scale coarse-grained beds, contrasting with darker, finer-grained beds, which display high %C values (Figure 10). Over the sampled interval, C/N weight ratios within cores from Campus Lagoon average 13.9, with values ranging between ~3 and ~24. Within Campus Lagoon, $\delta^{13}C_{org}$ averages -22‰ and ranges from -10‰ and -25‰. These shifts in $\delta^{13}C_{org}$ to less negative (closer to 0) values coincide with the appearance of cm-scale sand beds of facies SF2 as well as within the lower portions of MSF.

Within core AC15-01 from Las Salinas Lagoon, %C ranges from 0.2 wt% to 5.8 wt% (Figure 9). %C exhibits abrupt shifts to lower values within cm-scale sand beds of facies SF2 against higher values found within darker, fine-grained intervals of facies MFS. Over the sampled interval, C/N weight ratios within Las Salinas Lagoon average 12.4, with values ranging between ~5 and 34. Within this locality, $\delta^{13}C_{org}$ averages -23‰ and ranges from -12‰ to -25‰. Only 1 bed (76 – 90 cm) of sand of facies SF2 coincides with a large jump in $\delta^{13}C_{org}$ to less negative (closer to 0) values.

Data was further separated into groups based on facies assignment in order to compare values of $\delta^{13}C_{org}$ and $\delta^{15}N$ from Campus Lagoon and Las Salinas Lagoon to values obtained from modern depositional environments in the San Francisco Bay

area by Cloern et al. (2002). A cross plot of this data (Figure 11) displays clustering of data points associated with MSF, SF2 and SHF to $\delta^{13}C_{org}$ values between -17‰ and -24‰ and $\delta^{15}N$ values between 5‰ and 8‰. Data points associated with SF1 have $\delta^{13}C_{org}$ values between -19‰ and -25‰ with some outliers at -8‰ and $\delta^{15}N$ values between 3.7‰ and 5.5‰. Deposits associated with EF contain $\delta^{13}C_{org}$ values of -17‰ and $\delta^{15}N$ values of 10.4‰.

4.6) Subsidence and Uplift

Elevations of *C. californica* in cores from Las Salinas Lagoon provide late Holocene average subsidence rates of 0.278 ± 0.75 mm/yr (Figure 12; Table 3). In Campus lagoon, elevations of *C. californica* average negative rates of subsidence (-0.1 ± 0.9 mm/yr), indicating potential uplift (Figure 12; Table 3).

5) Discussion

5.1) Facies Interpretation

The six sedimentary facies identified in this study are interpreted to represent four major depositional environments. Changes in these facies through time are used to reconstruct the middle to late Holocene environmental history of Campus and Las Salinas Lagoons and provide insights as to how storms and earthquakes affected the Santa Barbara Channel coast through the Holocene. These environments include a shallow water high-energy lagoon, low energy lagoon, marine washover beds, and a coastal mudflat.

SF1: Shallow Water High-Energy Lagoon

The moderate sorting of coarse grains, the presence of ostracods *Cytheridae beaconensis*, prevalence of articulated bivalve shell material including *Tresus nuttalli* species, high CIA values (25), and bioturbation found within Sand Facies 1 (SF1) suggest a shallow sandy lagoon and/or subtidal sandflat environment. Deposits of this facies are similar to those found in the subtidal areas of the modern Batiquitos Lagoon and San Diego Bay (King et al., 2018; Scott et al., 2011). Beds of this facies display enriched values of $\delta^{15}N$, suggestive of autochthonous organic matter production rather than allocthonous aquatic marine organic matter, which traditionally has low $\delta^{15}N$ due to N-fixing algae (Page et al., 2008). The cross plot comparison (Figure 11) between isotope values from this study and those determined to represent modern environments in San Francisco, CA (Cloern et al., 2002) categorizes beds of this facies as dominated by estuarine-marine and C4 saltmarsh material.

MSF: Low Energy Lagoon

The finer grain size of the Muddy Silt Facies (MSF) suggests a low energy environment. The presence of foraminifera *Elphidium spp*., woody organic material, and shallow-water mollusk species suggest a protected lagoon or mudflat environment. The transition from articulated *Cardiidae* at its base to *Cerithidae* up core within this facies suggests the environment shifts from deeper open lagoon to a shallow mudflat. The cross plot of $\delta^{15}N$ vs $\delta^{13}C$ (Figure 11) categorizes beds of this facies as dominated by estuarine-marine and mudflat material.

A modern variant of this facies occurs at the top of cores extracted from within the lagoons. This modern MSF contains live roots and radiocarbon ages post 1950.

Based on the ongoing recent deposition of this modern MSF within the low energy lagoon environment, this environment is interpreted to represent conditions very similar to the modern lagoons.

EF & SHF: Coastal Mudflat

Found only within Campus Lagoon, the finer grain sizes of the Evaporite Facies (EF) suggest a low-energy environment. The presence of evaporite minerals displaying granular morphology indicate *in situ* growth of the gypsum within the mud rather than diagenetically occurring post deposition (Casby-Horton et al., 2015). These characteristics are indicative of an evaporative mudflat similar to modern environments described by Warren (1991). Below the bed of the EF facies in core CL16-01 is a distinct bed with fecal pellets and shell hash characterizing the shell hash facies (SHF). Shell Hash Facies (SHF) is interpreted to represent deposition originating from disturbance of the lagoonal environment. Evidence for disturbance includes an abundance of intertidal worm fecal pellet material within the bed of this facies and the transition from SF1 to SHF to Evaporite Facies (EF). The cross plot comparison (Figure 11) categorizes beds of this facies as dominated by C4 saltmarsh material.

5.2) Origin of Sand Beds (*SF2*)

The similarity in the sorting and mineralogy (dominantly quartz - ~80%) between Sand Facies 2 (SF2) and modern beach deposits suggests the sands of this facies are sourced from the beaches or shallow offshore environment (Figure 5). A marine source is supported by the presence of shell fragments, the seaward thickening of

these beds and, within Campus Lagoon, their increasing frequency in the more seaward portions of the lagoon (Figure 6).

Fine silt laminae are found along amalgamation surfaces in beds of SF2 within cores from Campus Lagoon. A storm overwash rather than aeolian origin is favored based on the range of grain sizes found within this facies. The grain-size of typical aeolian deposits is between 100 and 200 μm (Sun et al., 2002) while that of SF2 and beach sands is 200-400 μm. Plant material and shell fragments of *Tresus nuttalli* are observed within these deposits; however, the absence of roots suggests plant material is transported into the environment rather than from in-situ development.

Beds of SF2 display low values of $\delta^{15}N$, which in a lagoonal/marsh system is suggestive of allochthonous organic matter rather than autochthonous material, which traditionally has higher $\delta^{15}N$ due to organic matter derived from C3 plants (Peterson and Howarth, 1987). This shift towards allochthonous isotope signatures indicative of marine influence, as well as a lack of root material suggests beds of this facies are composed of material transported into the lagoon environment too fast for plant communities to become established and thus are likely the result of rapid marine incursion. The cross plot comparison (Figure 11) between isotope values from this study and those determined to represent modern environments in San Francisco, CA (Cloern et al., 2002) categorizes beds of this facies as incorporating estuarine-marine and soil/sediment material as well as deposition of estuarine marine and benthic diatom material in the cases of Las Salinas Lagoon and the seaward part of Campus Lagoon (CL13-01) respectively. This occurrence of low $\delta^{15}N$ values paired with estuarine $\delta^{13}C$ values is indicative of benthic diatom material by (Cloern et al., 2002)

and was also noted in intertidal flats after storm wave activity (Colijnl and Dijkema, 1981). SF2 beds are interpreted to represent marine washover due to their lateral continuity (Figure 6 & 7), the presence of marine shell fragments and marine organic material (kelp). In the case of Las Salinas Lagoon, a decrease in the presence of the terrestrial elemental metal aluminum, accompanied by an increase in calcium supports a marine washover origin.

The youngest beds of SF2 in Campus Lagoon range in age between 149 and 617 CYBP and may correlate to either the 1861-1862 flood (Reynolds et al., 2018) or older flood deposits observed in marine cores from the Santa Barbara Basin dated at 485 and 600 CYBP (Hendy et al., 2013; Du et al., 2018). The oldest bed of SF2 in core CL16-02, with a date range between 2581 and 4425 CYBP and a Bchron central age of 3400 CYBP, may correlate to the SF2 bed in Las Salinas Lagoon at 3300 ± 200 as well as a 3400 ± 200 CYBP flood deposit found in marine cores from the Santa Barbara Basin (Du et al., 2018). Large-scale, multi-decadal pluvial episodes are also recorded in Southern California at these times (Kirby et al., 2012) and may in part be related to more frequent AR storms. The presence of older beds of similar character, thickness and composition as the 1861-62 storm (Reynolds et al., 2018) suggest the storm was not unprecedented, but a reoccurring hazard along the California coast.

While the deepest of the three SF2 beds in Las Salinas Lagoon correlates with SF2 found in Campus Lagoon, the youngest two SF2 beds within Las Salinas Lagoon do not have equivalents within Campus Lagoon. However, they do overlap in age (Figure 13) with large magnitude earthquakes along the Pitas Point Ventura Avenue

thrust fault (Rockwell et al., 2016). Distinguishing tsunami and storm deposits is not a trivial task (Nanayama et al., 2000; Goff et al., 2004; Shanmugam, 2006; Morton et al., 2007). Previous studies have provided several suggestions for how to distinguish between these processes; however, these studies rely on modern, spatially relevant, examples of tsunami and storm deposits (Morton et al., 2007; Nanayama et al., 2000).

Distinguishing sedimentary characteristics of beds of SF2 compared to those of modern storm wave washover deposits (Morton et al., 2007) include an upwards fining, sharp basal contacts, and woody debris (Hutchinson and Clague, 2017) similar to tsunami deposits described from the Cascadia subduction zone (Atwater, 1987). These differences, especially the occurrence of woody debris as a result of outflow entrainment (Nanayama et al., 2000), can be attributed to dissimilarities in the hydrodynamics and transport sediment sorting processes between tsunami and storm processes (Morton et al., 2007). Beds of SF2 within Las Salinas Lagoon range in thickness from < 5 cm to > 30 cm, spanning the entire range of thicknesses characteristic of either tsunamis (<30cm) or storms (>30cm) (Morton et al., 2007). The two SF2 beds at 1100 ± 200 and 2200 ± 200 CYBP, contemporaneous with earthquake events, have thicknesses of 12 and 15 cm respectively suggesting they are the result of fewer than 10 overland waves and likely occurring in minutes to hours, rather than hours to days (Gelfenbaum and Jaffe, 2003). The overall similarity of the two beds of SF2 at 1100 ± 200 and 2200 ± 200 CYBP as well as their coincident timing with large earthquake events suggests these beds within Las Salinas Lagoon may be the result of tsunamis rather than storm derived washover.

Dynamic models from Ryan et al. (2015) suggest the Pitas Point Ventura Avenue Thrust Fault has the potential to generate tsunamis between 5 and 6 m in amplitude in the Santa Barbara region. According to the model results of (Ryan et al., 2015), the tsunami should be much larger in Las Salinas Lagoon than either Campus Lagoon or neighboring Devereux Slough (7 m versus 3 m), which may explain its absence in those two lagoons located farther to the west (Nelson, 2018). However, one would expect to find evidence for the tsunami if it occurred in Carpinteria Slough to the east of Las Salinas Lagoon and directly onshore from the proposed fault rupture (Ryan et al., 2015). However, studies in Carpinteria Slough provide no evidence for marine overwash at this time, despite attempts to identify them (Reynolds, 2018).

In other systems, such are those in the Cascadia subduction zone described in Atwater (1987), tsunami presence and deposition is enhanced by co-seismic subsidence. Considering Las Salinas Lagoon's location within a subsiding synclinal basin reflected in its signal of long-term subsidence (Figure 12), accompanied by a transition from beds of MSF with shallower water fauna below SF2 beds to deeper water fauna within MSF above SF2 beds (Figure 7), may suggest that Las Salinas Lagoon subsides co-seismically with the Pitas Point Ventura Avenue Thrust Fault (Figure 13); however, the low number of faunal specimens within beds of MSF prevents a conclusive test of the co-seismic subsidence hypothesis.

5.3) Santa Barbara Channel climate and geomorphology at significant intervals

Masters (2006) established a proxy record of sand beach accretion in Southern California for the past 10 ka using radiocarbon dates of *Tivela stultorum*, a common beach clam. This record reflects a ~7000 CYBP flux of sand, deposited into the Santa Barbara Littoral Cell resulting in the formation of sand beaches along the coastline (Masters, 2006). Dominant La Niña conditions from 7000 to 5000 CYBP (Moy et al., 2002) brought oblique-to-coast wave energy, as a result of northwest wave direction from Aleutian low pressure systems, providing protection to drowned river valleys and the establishment of beaches at the mouth of estuaries and lagoons. These beaches isolated these systems from waves and ocean conditions.

The *Tivela* record shows a major transition in the Santa Barbara coast between 4600 and 5000 CYBP when perennial sand beaches were lost or extensively depleted (Figure 13, Masters, 2006). This transition to more vulnerable estuary and lagoon environments coincides with the intensification of El Niño events (Figure 13) and floods in Southern California (Moy et al., 2002; Schimmelmann et al., 2003; Masters, 2006). Storms track farther south during El Niño winters in Southern California compared to La Niña periods, generating higher waves and eroding established beaches (Ludka et al., 2016). This erosion may have led to an increase in ocean influence and marine disturbance within estuaries and lagoons as the baymouth barrier and beaches isolating them from the ocean were destroyed helping to establish the environments represented by facies SF1 (Figure 13). The period of less frequent El Niño events that followed from 4600 to 3800 CYBP as well as a contemporaneous reduction in the rate of sea-level rise may have allowed the redevelopment of beaches and the formation of barrier-bars in front of the estuaries, resulting in the transition to

calmer environments and the deposition of MSF and EF behind the barrier-bars (Masters and Flemming, 1983; Orme, 2002).

The ages of the beds of SF2 found in Las Salinas Lagoon at 1100 ± 200 and 2200 ± 200 CYBP do not correlate with major pluvials or flood deposits recording in other southern California archives (Kirby et al., 2012; Moy et al., 2002; Du et al., 2018). This disagreement further supports a non-storm origin for the overwash processes responsible for the deposition of these beds, further supporting a tsunami origin for these beds.

5.4) Intervals of storm recurrence

Corroborating marine washover beds of SF2 with proxies of pluvial events in California (Kirby et al., 2012) and flood layers found within the Santa Barbara Channel (Du et al., 2018) we should expect large scale pluvials and floods to coincide with periods of SF2 deposition. The record from Bear Lake, CA (Kirby et al., 2012) records major pluvials at 476-500, 700-850, and 3000-3350 CYBP largely coinciding with the deposition of major flood layers in the Santa Barbara Channel at 400, 780, and 3380 CYBP (Du et al., 2018). SF2 deposits from Campus Lagoon and Las Salinas Lagoon dated to 388 ±41, 617 ± 105 and 3400 ±190 CYBP (Table 2) are broadly consistent with recorded pluvial episodes and flood deposits.

Assuming all deposits of SF2 (including those from Las Salinas Lagoon) are the result of storm wave washover (Ockham's razor), a recurrence interval may be established for storms similar or greater in magnitude than that experienced in 1861-1862. Based on all deposits described, storms of this magnitude are hypothesized to

occur along the Santa Barbara coastline every 660 years (Figure 14); however, when calculating rates based on storm beds post 2000 CYBP, a recurrence interval of 320 years is established. If the two SF2 beds from Las Salinas Lagoon that may represent tsunami deposits are not included, this recurrence interval is reduced to 1066 years, again shifting to a recurrence interval of 320 years post 550 CYBP. This apparent doubling of the storm frequency may be a response to more frequent El Niño events as well as a climate regime comprised of consistent pluvials. The California recurrence interval of large storms, post 2000 CYBP, based on sediment layers in the Santa Barbara Basin (Du et al., 2018) as well as from tidal marshes in San Francisco Bay (Malamud-Roam and Ingram, 2004) is ~280 years (Dettinger and Ingram, 2013) (Figure 14). The similarity in recurrence intervals between our study and that of Dettinger and Ingram (2013) further suggests coastal estuarine and lagoon systems may provide valuable records of frequency of storms.

The distinct difference between recurrence intervals pre and post 2000 CYBP may be the result of two processes: A) Larger beaches, extending the shoreline farther seaward resulting in a higher threshold, with regards to the size of storms, for preservation to occur. B) A change in storm recurrence driven by climatic changes occurred along the West coast of North America. Future work should further investigate these two hypotheses to better understand the relationship between storm frequency and climate regime.

5.5) Coastal Subsidence

The patterns of subsidence and uplift within Las Salinas and Campus Lagoons, respectively, fit their general geological settings. Las Salinas Lagoon lies within a subsiding synclinal basin bound by three reverse faults (Mission Ridge Fault, Mesa Fault, and Cemetery Fault). A subsidence rate of 0.278 ± 0.75 m/kyr (Figure 12) fits this geological setting. Conversely, Campus Lagoon is found on the upthrown side of the More Ranch Fault within a stream valley incised in a MIS3 marine terrace (Gurrola et al., 2014). The uplift of the lagoon at a rate of 0.1 ± 0.9 m/kyr fits that general geological setting (Figure 2).

5.6) Tectonic Implications

The structure and fault systems of the SBFTB are still debated (Marshall et al., 2017). Mechanical models (Marshall et al., 2017; Plesch et al., 2007) suggest that the subsurface geometry of the Pitas Point Fault is either of a "ramp" or "no-ramp" structure, which would induce uplift in discrete events or gradually, respectively. The two end member fault models predict different rupture scenarios during earthquakes and hence tsunami potentials. Models using a ramp geometry are capable of creating a significant tsunami while those with a no-ramp geometry are not (Ryan et al., 2015). If the two beds of SF2 deposits within Las Salinas Lagoon are the result of tsunami overwash, that would support models calling for a ramp geometry for the Pitas Point Fault.

6) Conclusion

Nine cores from two lagoons along the Northern Santa Barbara Channel coast reveal aspects of the geological and environmental history of the region over the last 4800 years. This study identified five sedimentary facies defining four depositional environments. Five major groups of sand beds were identified between the two lagoons, and were interpreted to represent multiple atmospheric river storms and 2 possible tsunami events. These storm beds date to <149 CYBP, 388 ±41 CYBP, 617 ± 105 CYBP in Campus Lagoon and 3400 ±190 CYBP within both Campus and Las Salinas Lagoons, while beds at 1050 ± 200 CYBP and 2250 ± 300 CYBP within Las Salinas Lagoon lithologically similar to the aforementioned storm beds, are coincident with large earthquakes along the Pitas Point Thrust and may represent tsunami deposits. The frequency of overwash beds within Campus Lagoon suggests a recurrence interval of 660 years based on the assumption that all of the overwash beds represent storm washover, while a shift in the recurrence interval to 320 years, comparable to that of other Californian studies, is observed at 2000 CYBP. An across-system transition from a subtidal sandy lagoon (SF1) to a shallow lagoonal environment (MSF) likely represents the progradation of sand beaches and the establishment of barrier-bars and the creation of back-barrier estuaries along the Santa Barbara Channel in response to a transition from El Niño to La Niña dominant conditions and a reduction in the rate of sea-level rise around 4400 CYBP. Rapid transitions observed between facies in both lagoons suggest climate shifts between El Niño/La Niña frequency and possibly seismicity play roles as drivers of environmental change along the Santa Barbara Channel coastline.

References

Atwater, B.F., 1987, Evidence for great holocene earthquakes along the outer coast of washington state.: Science (New York, N.Y.), v. 236, p. 942–4, doi: 10.1126/science.236.4804.942.

Bird, B.W., and Kirby, M.E., 2006, An alpine lacustrine record of early Holocene North American Monsoon dynamics from Dry Lake, southern California (USA): Journal of Paleolimnology, doi: 10.1007/s10933-005-8514-3.

Borrero, J.C., Legg, M.R., and Synolakis, C.E., 2004, Tsunami sources in the southern California bight: Geophysical Research Letters, v. 31, p. n/a-n/a, doi: 10.1029/2004GL020078.

Boyles, J., Scott, A., and Rine, J., 1986, A logging form for graphic descriptions of core and outcrop: journal of sedimentary petrology, v. 56, p. 567–568.

Casby-Horton, S., Herrero, J., and Rolong, N.A., 2015, Gypsum Soils—Their Morphology, Classification, Function, and Landscapes: Advances in Agronomy, v. 130, p. 231–290, doi: 10.1016/BS.AGRON.2014.10.002.

Cayan, D.R., Redmond, K.T., Riddle, L.G., Cayan, D.R., Redmond, K.T., and Riddle, L.G., 1999, ENSO and Hydrologic Extremes in the Western United States*: http://dx.doi.org/10.1175/1520-0442(1999)012<2881:EAHEIT>2.0.CO;2, doi: 10.1175/1520-0442(1999)012<2881:EAHEIT>2.0.CO;2.

Cloern, J.E., Canuel, E.A., and Harris, D., 2002, Stable carbon and nitrogen isotope composition of aquatic and terrestrial plants of the San Francisco Bay estuarine system: Limnology & Oceanography, v. 47, p. 713–729, doi: 10.4319/lo.2002.47.3.0713.

Colijnl, F., and Dijkema, K.S., 1981, Species Composition of Benthic Diatoms and Distribution of Chlorophyll a on an Intertidal Flat in the Dutch Wadden Sea: Marine Ecology Progress Series, v. 4, http://www.int-res.com/articles/meps/4/m004p009.pdf (accessed April 2018).

Cook, B.I., Seager, R., and Miller, R.L., 2011, Atmospheric circulation anomalies during two persistent north american droughts: 1932–1939 and 1948–1957: Climate Dynamics, v. 36, p. 2339–2355, doi: 10.1007/s00382-010-0807-1.

Dettinger, M., 2011, Climate change, atmospheric rivers, and floods in California - a multimodel analysis of storm frequency and magnitude changes: Journal of the American Water Resources Association, doi: 10.1111/j.1752-1688.2011.00546.x.

Dettinger, M.D., and Ingram, B.L., 2013, THE COMING MEGAFLOODS: Source: Scientific American, v. 308, p. 64–71, http://www.jstor.org/stable/26017895 (accessed May 2018).

Dettinger, M.D., Ralph, F.M., Das, T., Neiman, P.J., and Cayan, D.R., 2011, Atmospheric Rivers, Floods and the Water Resources of California: Water, doi: 10.3390/w3020445.

Dibblee, T.W., 1966, Geology of the Central Santa Ynez Mountains, Santa Barbara County, California: California Division of Mines and Geology Bulletin 186, 1-

99 p.
Dingemans, T., Mensing, S.A., Feakins, S.J., Kirby, M.E., and Zimmerman, S.R.H., 2014, 3000 years of environmental change at Zaca Lake, California, USA: Frontiers in Ecology and Evolution, doi: 10.3389/fevo.2014.00034.
Du, X., Hendy, I., and Schimmelmann, A., 2018, A 9000-year flood history for Southern California: A revised stratigraphy of varved sediments in Santa Barbara Basin: Marine Geology, v. 397, p. 29–42, doi: 10.1016/J.MARGEO.2017.11.014.
Ejarque, A., Anderson, R.S., Simms, A.R., and Gentry, B.J., 2015, Prehistoric fires and the shaping of colonial transported landscapes in southern California: A paleoenvironmental study at Dune Pond, Santa Barbara County: Quaternary Science Reviews, v. 112, p. 181–196, doi: 10.1016/j.quascirev.2015.01.017.
Engstrom, W., 1996, The California storm of January 1862: Quaternary Research, doi: 10.1006/qres.1996.0054.
Fye, F.K., Stahle, D.W., Cook, E.R., Fye, F.K., Stahle, D.W., and Cook, E.R., 2009, Twentieth-Century Sea Surface Temperature Patterns in the Pacific during Decadal Moisture Regimes over the United States*: http://dx.doi.org/10.1175/1087-3562(2004)8<1:TSSTPI>2.0.CO;2, doi: 10.1175/1087-3562(2004)8<1:TSSTPI>2.0.CO;2.
Gelfenbaum, G., and Jaffe, B., 2003, Erosion and Sedimentation from the 17 July, 1998 Papua New Guinea Tsunami: Pure and Applied Geophysics, v. 160, p. 1969–1999, doi: 10.1007/s00024-003-2416-y.
Gesch, D.B., 2002, The National Elevation Dataset:, https://topotools.cr.usgs.gov/pdfs/Gesch_Chp_4_Nat_Elev_Data_2007.pdf (accessed April 2018).
Goff, J., McFadgen, B.G., and Chagué-Goff, C., 2004, Sedimentary differences between the 2002 Easter storm and the 15th-century Okoropunga tsunami, southeastern North Island, New Zealand: Marine Geology, v. 204, p. 235–250, doi: 10.1016/S0025-3227(03)00352-9.
Gulbranson, E.L., Montañez, I.P., Tabor, N.J., and Montañ Ez, I.P., 2011, A Proxy for Humidity and Floral Province from Paleosols A RT I C L E S A Proxy for Humidity and Floral Province from Paleosols: Source: The Journal of GeologyThe Journal of Geology, v. 119, p. 559–573, doi: 10.1086/661975.
Gurrola, L.D., Keller, E.A., Chen, J.H., Owen, L.A., and Spencer, J.Q., 2014, Tectonic geomorphology of marine terraces: Santa Barbara fold belt, California: Bulletin of the Geological Society of America, v. 126, p. 219–233, doi: 10.1130/B30211.1.
Haslett, J., and Parnell, A., 2008, A simple monotone process with application to radiocarbon-dated depth chronologies: Journal of the Royal Statistical Society. Series C: Applied Statistics, doi: 10.1111/j.1467-9876.2008.00623.x.
Hendy, I.L., Dunn, L., Schimmelmann, A., and Pak, D.K., 2013, Resolving varve and radiocarbon chronology differences during the last 2000 years in the Santa Barbara Basin sedimentary record, California: Quaternary International, doi: 10.1016/j.quaint.2012.09.006.
Holmquist, J.R., Reynolds, L., Brown, L.N., Southon, J.R., Simms, A.R., and

MacDonald, G.M., 2015, Marine Radiocarbon Reservoir Values in Southern California Estuaries: Interspecies, Latitudinal, and Interannual Variability: Radiocarbon, v. 57, p. 449–458, doi: 10.2458/azu_rc.57.18389.
Hurteau, M., Zald, H., and North, M., 2007, Species-specific response to climate reconstruction in upper-elevation mixed-conifer forests of the western Sierra Nevada, California: Canadian Journal of Forest Research, v. 37, p. 1681–1691, doi: 10.1139/X07-028.
Hutchinson, I., and Clague, J., 2017, Were they all giants? Perspectives on late Holocene plate-boundary earthquakes at the northern end of the Cascadia subduction zone: Quaternary Science Reviews, v. 169, p. 29–49, doi: 10.1016/J.QUASCIREV.2017.05.015.
Inman, D.L., Masters, P.M., and Jenkins, S.A., 2005, Facing the Coastal Challenge: Modeling Coastal Erosion in Southern California, *in* California and the World Ocean '02, Reston, VA, American Society of Civil Engineers, p. 38–52, doi: 10.1061/40761(175)4.
Johnson, S.Y., Hartwell, S.R., Sorlien, C.C., Dartnell, P., and Ritchie, A.C., 2017, Shelf evolution along a transpressive transform margin, Santa Barbara Channel, California: Geosphere, v. 13, doi: 10.1130/GES01387.1.
de Jong, R., Björck, S., Björkman, L., and Clemmensen, L.B., 2006, Storminess variation during the last 6500 years as reconstructed from an ombrotrophic peat bog in Halland, southwest Sweden: Journal of Quaternary Science, doi: 10.1002/jqs.1011.
Keller, E.A., and DeVecchio, D.E., 2013, Tectonic geomorphology of active folding and development of transverse drainages, *in* Treatise on Geomorphology, San Diego, CA, Academic Press, p. 129–147.
Keller, E.A., and Gurrola, L.D., 2000, NEHRP Final Report: Earthquake Hazard of the Santa Barbara Fold Belt California: Institute for Crustal Studies, University of California Santa Barbara, p. 1–108.
Kennett, D.J., Kennett, J.P., Erlandson, J.M., and Cannariato, K.G., 2007, Human responses to Middle Holocene climate change on California's Channel Islands: Quaternary Science Reviews, v. 26, p. 351–367, doi: 10.1016/j.quascirev.2006.07.019.
King, B.L., Simms, A.R., and Simkins, L.M., 2017, THE STRATIGRAPHIC ARCHITECTURE OF SMALL INCISED VALLEYS ALONG AN ACTIVE MARGIN : EXAMPLES FROM THE OCEANSIDE LITTORAL CELL OF THE SOUTHERN CALIFORNIA COAST: Society for Sedimentary Geology special publication, p. 1–10, doi: 10.2110/sepmsp.108.02.
Kirby, M.E., Lund, S.P., Anderson, M.A., and Bird, B.W., 2007, Insolation forcing of Holocene climate change in Southern California: a sediment study from Lake Elsinore: Journal of Paleolimnology, v. 38, p. 395–417, doi: 10.1007/s10933-006-9085-7.
Kirby, M.E., Lund, S.P., Patterson, W.P., Anderson, M.A., Bird, B.W., Ivanovici, L., Monarrez, P., and Nielsen, S., 2010, A Holocene record of Pacific Decadal Oscillation (PDO)-related hydrologic variability in Southern California (Lake Elsinore, CA): Journal of Paleolimnology, doi: 10.1007/s10933-010-9454-0.
Kirby, M.E., Zimmerman, S.R.H., Patterson, W.P., and Rivera, J.J., 2012, A 9170-

year record of decadal-to-multi-centennial scale pluvial episodes from the?coastal Southwest United States: a role for atmospheric rivers? Quaternary Science Reviews, v. 46, p. 57–65, doi: 10.1016/j.quascirev.2012.05.008.
Li, C., and Yang, S., 2010, Is chemical index of alteration (CIA) a reliable proxy for chemical weathering in global drainage basins? American Journal of Science, v. 310, p. 111–127, doi: 10.2475/02.2010.03.
Ludka, B.C., Gallien, T.W., Crosby, S.C., and Guza, R.T., 2016, Mid-El Niño erosion at nourished and unnourished Southern California beaches: Geophysical Research Letters, v. 43, p. 4510–4516, doi: 10.1002/2016GL068612.
Malamud-Roam, F., and Lynn Ingram, B., 2004, Late Holocene ??13C and pollen records of paleosalinity from tidal marshes in the San Francisco Bay estuary, California: Quaternary Research, doi: 10.1016/j.yqres.2004.02.011.
Marshall, S.T., Funning, G.J., Krueger, H.E., Owen, S.E., and Loveless, J.P., 2017, Mechanical models favor a ramp geometry for the Ventura-pitas point fault, California: Geophysical Research Letters, v. 44, p. 1311–1319, doi: 10.1002/2016GL072289.
Masters, P.M., 2006, Holocene sand beaches of southern California: ENSO forcing and coastal processes on millennial scales: Palaeogeography, Palaeoclimatology, Palaeoecology, v. 232, p. 73–95, doi: 10.1016/J.PALAEO.2005.08.010.
Masters, P., and Flemming, N., 1983, Quaternary Coastlines and Marine Archaeology: Geoarchaeology, v. 1, p. 313–315, doi: 10.1002/gea.3340010309.
Minor, S.A., Kellog, K.S., Stanley, R.G., Gurrola, L.D., Keller, E.A., and Brandt, T.R., 2009, Geologic Map of the Santa Barbara Coastal Plain Area, Santa Barbara County, California: USGS,.
Morton, R.A., Gelfenbaum, G., and Jaffe, B.E., 2007, Physical criteria for distinguishing sandy tsunami and storm deposits using modern examples: Sedimentary Geology, doi: 10.1016/j.sedgeo.2007.01.003.
Moy, C.M., Seltzer, G.O., Rodbell, D.T., and Anderson, D.M., 2002, Variability of El Niño/Southern Oscillation activity at millennial timescales during the Holocene epoch: Nature, v. 420, p. 162–165, doi: 10.1038/nature01194.
Namias, J., Yuan, X., Cayan, D.R., Namias, J., Yuan, X., and Cayan, D.R., 1988, Persistence of North Pacific Sea Surface Temperature and Atmospheric Flow Patterns: http://dx.doi.org/10.1175/1520-0442(1988)001<0682:PONPSS>2.0.CO;2, doi: 10.1175/1520-0442(1988)001<0682:PONPSS>2.0.CO;2.
Nanayama, F., Shigeno, K., Satake, K., Shimokawa, K., Koitabashi, S., Miyasaka, S., and Ishii, M., 2000, Sedimentary differences between the 1993 Hokkaido-nansei-oki tsunami and the 1959 Miyakojima typhoon at Taisei, southwestern Hokkaido, northern Japan: Sedimentary Geology, v. 135, p. 255–264, doi: 10.1016/S0037-0738(00)00076-2.
Neiman, P.J., Ralph, F.M., Moore, B.J., Hughes, M., Mahoney, K.M., Cordeira, J.M., and Dettinger, M.D., 2013, The Landfall and Inland Penetration of a Flood-Producing Atmospheric River in Arizona. Part I: Observed Synoptic-Scale,

Orographic, and Hydrometeorological Characteristics: Journal of Hydrometeorology, v. 14, p. 460–484, doi: 10.1175/JHM-D-12-0101.1.
Nelson, Z., 2018, Late pleistocene to holocene environmental history of devereux slough: University of California Santa Barbara.
Nesbitt, H.W. Young, G.M., 1982, Early Proterozoic climates and plate motions inferred from major elemenet chemistry of lutites: Nature, v. 299, p. 715–717.
Noren, A.J., Bierman, P.R., Steig, E.J., Lini, A., and Southon, J., 2002, Millennial-scale storminess variability in the northeastern United States during the Holocene epoch: Nature, doi: 10.1038/nature01132.
Olsson, I., and Berglund, B., 1986, Handbook of Holocene palaeoecolgy and palaeohydrology: John Wiley & Sons, 273-312 p.
Orme, A.R., 2002, Ocean coasts and continental margins, *in* The Physical Geography of North America, Oxford University Press, p. 425–455.
Osleger, D.A., Heyvaert, A.C., Stoner, J.S., and Verosub, K.L., 2009, Lacustrine turbidites as indicators of Holocene storminess and climate: Lake Tahoe, California and Nevada: Journal of Paleolimnology, doi: 10.1007/s10933-008-9265-8.
Page, H., Reed, D., Brzezinski, M., Melack, J., and Dugan, J., 2008, Assessing the importance of land and marine sources of organic matter to kelp forest food webs: Marine Ecology Progress Series, v. 360, p. 47–62, http://ucelinks.cdlib.org:8888/sfx_local?genre=article&epage=62&volume=360&pages=47-62&title=Marine+Ecology+Progress+Series&date=2008-05-22&sid=jstor%3Ajstor&spage=47&eissn=16161599&atitle=Assessing+the+importance+of+land+and+marine+sources+of+organic+mat (accessed January 2018).
Parnell, A.C., Buck, C.E., and Doan, T.K., 2011, A review of statistical chronology models for high-resolution, proxy-based Holocene palaeoenvironmental reconstruction: Quaternary Science Reviews, doi: 10.1016/j.quascirev.2011.07.024.
Patch, K., and Griggs, G., 2006, Littoral Cells, Sand Budgets, and Beaches: Understanding California's Shoreline: University of California Santa Barbara.
Peterson, B.J., and Howarth, R.W., 1987, Sulfur, carbon, and nitrogen isotopes used to trace organic matter flow in the salt-marsh estuaries of Sapelo Island, Georgia1: Limnology and Oceanography, v. 32, p. 1195–1213, doi: 10.4319/lo.1987.32.6.1195.
Plesch, A., Shaw, J.H., Benson, C., Bryant, W.A., Carena, S., Cooke, M., Dolan, J., Fuis, G., Gath, E., Grant, L., Hauksson, E., Jordan, T., Kamerling, M., Legg, M., et al., 2007, Community Fault Model (CFM) for Southern California: Bulletin of the Seismological Society of America, v. 97, p. 1793–1802, doi: 10.1785/0120050211.
Pyke, C.B., and Bedell, C., 1972, Some Meteorological Aspects of the Seasonal Distribution of Precipitation in the Western United States and Baja California.: Thesis (PH.D.)--UNIVERSITY OF CALIFORNIA, LOS ANGELES, 1972.Source: Dissertation Abstracts International, Volume: 33-03, Section:

B, page: 1235., http://adsabs.harvard.edu/abs/1972PhDT.....35P (accessed September 2017).
Ralph, F.M., Neiman, P.J., Wick, G.A., Gutman, S.I., Dettinger, M.D., Cayan, D.R., and White, A.B., 2006, Flooding on California's Russian River: Role of atmospheric rivers: Geophysical Research Letters, doi: 10.1029/2006GL026689.
Reimer, P., Bard, E., Bayliss, A., Beck, J., Blackwell, P., Ramsey, C., Buck, C., Cheng, H., Edwards, R., Friedrich, M., Grootes, P., Guilderson, T., Haflidason, H., Hajdas, I., et al., 2013, Intcal13 and marine13 radiocarbon age calibration curves 0 – 50,000 years cal bp: Radiocarbon, doi: 10.2458/rc.v51i4.3569.
Reynolds, L.C., 2018, The late quaternary evolution of the southern california coast: Sea-level change, storms, and subsidence: University of California Santa Barbara.
Reynolds, L.C., and Simms, A.R., 2015, Late Quaternary relative sea level in Southern California and Monterey Bay: Quaternary Science Reviews, v. 126, p. 57–66, doi: 10.1016/j.quascirev.2015.08.003.
Reynolds, L.C., Simms, A.R., Ejarque, A., King, B., Anderson, R.S., Carlin, J.A., Bentz, J.M., Rockwell, T.K., and Peters, R., 2018, Coastal flooding and the 1861-2 California storm season: Marine Geology, v. 400, p. 49–59, doi: 10.1016/J.MARGEO.2018.02.005.
Rockwell, T.K., Clark, K., Gamble, L., Oskin, M.E., Haaker, E.C., and Kennedy, G.L., 2016, Large Transverse Range Earthquakes Cause Coastal Upheaval near Ventura, Southern California: Bulletin of the Seismological Society of America, v. 106, p. 2706–2720, doi: 10.1785/0120150378.
Rubin, C.M., Sieh, K., Chen, Y.-G., Lee, J.-C., Chu, H.-T., Yeats, R., Mueller, K., and Chan, Y.-C., 2001, Surface rupture and behavior of thrust faults probed in Taiwan: Eos, Transactions American Geophysical Union, v. 82, p. 565–565, doi: 10.1029/01EO00331.
Ryan, K.J., Geist, E.L., Barall, M., and Oglesby, D.D., 2015, Dynamic models of an earthquake and tsunami offshore Ventura, California: Geophysical Research Letters, v. 42, p. 6599–6606, doi: 10.1002/2015GL064507.
San Francisco Estuary Institute U.S. Coast Survey Maps of California - Southern California Coast T-Sheets (1851-1889):, http://www.caltsheets.org/socal/download.html (accessed April 2018).
Schimmelmann, A., Lange, C.B., and Meggers, B.J., 2003, Palaeoclimatic and archaeological evidence for a 200-yr recurrence of floods and droughts linking California, Mesoamerica and South America over the past 2000 years: The Holocene, v. 13, p. 763–778, doi: 10.1191/0959683603hl661rp.
Scholz, D., Hoffmann, D.L., Hellstrom, J., and Bronk Ramsey, C., 2012, A comparison of different methods for speleothem age modelling: Quaternary Geochronology, doi: 10.1016/j.quageo.2012.03.015.
Scott, D.B., Mudie, P.J., and Bradshaw, J.S., 2011, COASTAL EVOLUTION OF SOUTHERN CALIFORNIA AS INTERPRETED FROM BENTHIC FORAMINIFERA, OSTRACODES, AND POLLEN: Journal of Foraminiferal Research, v. 41, http://jfr.geoscienceworld.org/content/41/3/285 (accessed June 2017).

Shanmugam, G., 2006, The Tsunamite Problem: Journal of Sedimentary Research, v. 76, p. 718–730, doi: 10.2110/jsr.2006.073.
Sheldon, N.D., Retallack, G.J., and Tanaka, S., 2002, Geochemical Climofunctions from North American Soils and Application to Paleosols across the Eocene-Oligocene Boundary in Oregon: Source: The Journal of Geology, v. 110, p. 687–696, doi: 10.1086/342865.
Shields, C.A., and Kiehl, J.T., 2016, Atmospheric river landfall-latitude changes in future climate simulations: Geophysical Research Letters, v. 43, p. 8775–8782, doi: 10.1002/2016GL070470.
Shin, H.H., LI, Z., Kim, Y.-O., Jung, S.W., Han, M.-S., Lim, W., and Yoon, Y.H., 2014, Morphological features and viability of Scrippsiella trochoidea cysts isolated from fecal pellets of the polychaete Capitella sp.: Harmful Algae, v. 37, p. 47–52, doi: 10.1016/j.hal.2014.05.005.
Simms, A., Reynolds, L.C., Bentz, M., Roman, A., Rockwell, T., and Peters, R., 2016, Tectonic Subsidence of California Estuaries Increases Forecasts of Relative Sea-Level Rise: Estuaries and Coasts, v. 39, p. 1571–1581, doi: 10.1007/s12237-016-0105-1.
Sousa, W.P., 1983, Host life history and the effect of parasitic castration on growth: A field study of Cerithidea californica Haldeman (Gastropoda : Prosobranchia) and its trematode parasites: Journal of Experimental Marine Biology and Ecology, v. 73, p. 273–296, doi: 10.1016/0022-0981(83)90051-5.
Sperazza, M., Moore, J.N., and Hendrix, M.S., 2004, High-Resolution Particle Size Analysis of Naturally Occurring Very Fine-Grained Sediment Through Laser Diffractometry: Journal of Sedimentary Research, doi: 10.1306/031104740736.
Stuiver, M., and Reimer, P.J., 1993, Extended 14C Data Base and Revised CALIB 3.0 14C Age Calibration Program: Radiocarbon, v. 35, p. 215–230, doi: 10.1017/S0033822200013904.
Stuiver, M., Reimer, paula J., and Brazinas, T.F., 1998, HIGH-PRECISION RADIOCARBON AGE CALIBRATION FOR TERRESTRIAL AND MARINE SAMPLES: RADIOCARBON, v. 40, p. 1127–1151, https://journals.uair.arizona.edu/index.php/radiocarbon/article/viewFile/3786/3211 (accessed October 2017).
Sullivan, D.G., Byrne, R., Cowart, A., and Zimmerman, S., 2015, A record of late Holocene paleomegafloods from Little Packer Lake and Razor Slough, Sacramento valley oxbow Lakes: Quaternary International, v. 387, p. 147, doi: 10.1016/J.QUAINT.2015.01.179.
Sun, D., Bloemendal, J., Rea, D.., Vandenberghe, J., Jiang, F., An, Z., and Su, R., 2002, Grain-size distribution function of polymodal sediments in hydraulic and aeolian environments, and numerical partitioning of the sedimentary components: Sedimentary Geology, v. 152, p. 263–277, doi: 10.1016/S0037-0738(02)00082-9.
Trenberth, K.E., and Hurrell, J.W., 1994, Decadal atmosphere-ocean variations in the Pacific: Climate Dynamics, v. 9, p. 303–319, doi: 10.1007/BF00204745.
Upson, J.E., 1951, Former marine shore lines of the Gaviota Quadrangle, Santa

Barbara County, California: Journal of Geology, v. 59, p. 415–446.
Waliser, D., and Guan, B., 2017, Extreme winds and precipitation during landfall of atmospheric rivers: Nature Geoscience, doi: 10.1038/ngeo2894.
Warren, J.K., 1991, Chapter 2 Sulfate Dominated Sea-Marginal and Platform Evaporative Settings:: Sabkhas and Salinas, Mudflats and Salterns: Developments in Sedimentology, v. 50, p. 69–187, doi: 10.1016/S0070-4571(08)70260-7.
Wright, A.J., Edwards, R.J., van de Plassche, O., Blaauw, M., Parnell, A.C., van der Borg, K., de Jong, A.F.M., Roe, H.M., Selby, K., and Black, S., 2017, Reconstructing the accumulation history of a saltmarsh sediment core: Which age-depth model is best? Quaternary Geochronology, v. 39, p. 35–67, doi: 10.1016/J.QUAGEO.2017.02.004.
Zhu, Y., and Newell, R.E., 1998, A Proposed Algorithm for Moisture Fluxes from Atmospheric Rivers: Monthly Weather Review, doi: 10.1175/1520-0493(1998)126<0725:APAFMF>2.0.CO;2.
Zong, Y., and Sawai, Y., 2015, Diatoms, *in* Handbook of Sea-Level Research, Chichester, UK, John Wiley & Sons, Ltd, p. 233–248, doi: 10.1002/9781118452547.ch15.

Appendix

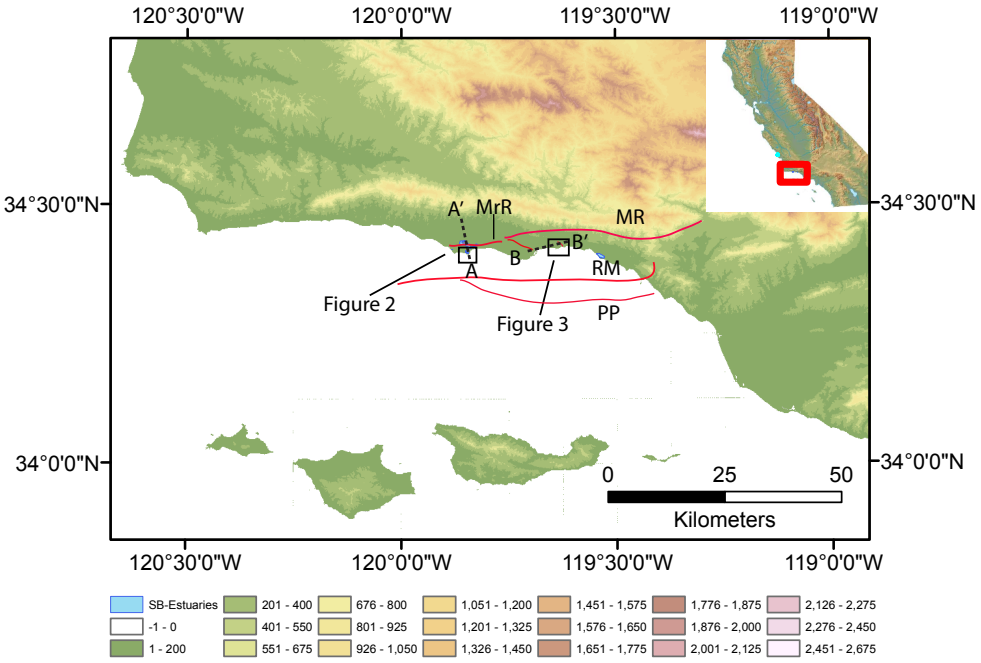

Figure 1: Digital elevation model (Gesch, 2002) of the region surrounding the Santa Barbara Channel displaying the general location of the study sites (black boxes). Inset shows the location of the Santa Barbara Channel region with respect to the state of California. Major faults discussed in text are shown. MrR) More Ranch Fault. MR) Mission Ridge Fault. RM) Red Mountain Fault. PP) Pitas Point Fault. Fault locations are based on (Keller and Gurrola, 2000). Dashed lines denote cross section locations for Figures 2 and 3.

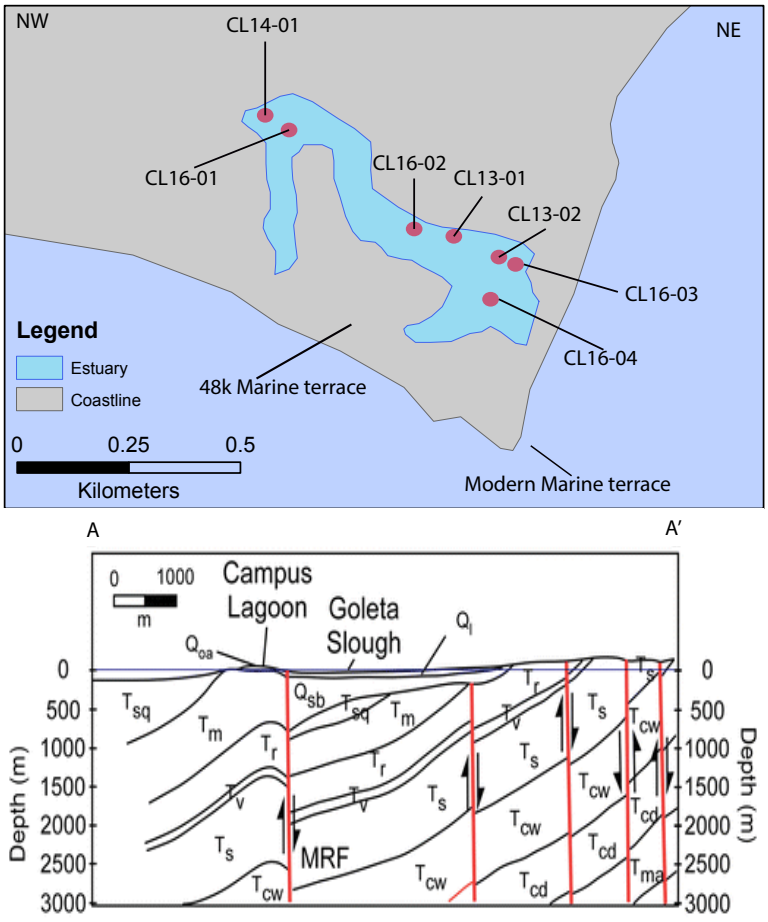

Figure 2: Map of the core locations (pink circles) within Campus Lagoon. See Figure 1 for general location. Lower cross section from Dibblee 1966. Reference cross section from Figure 1.

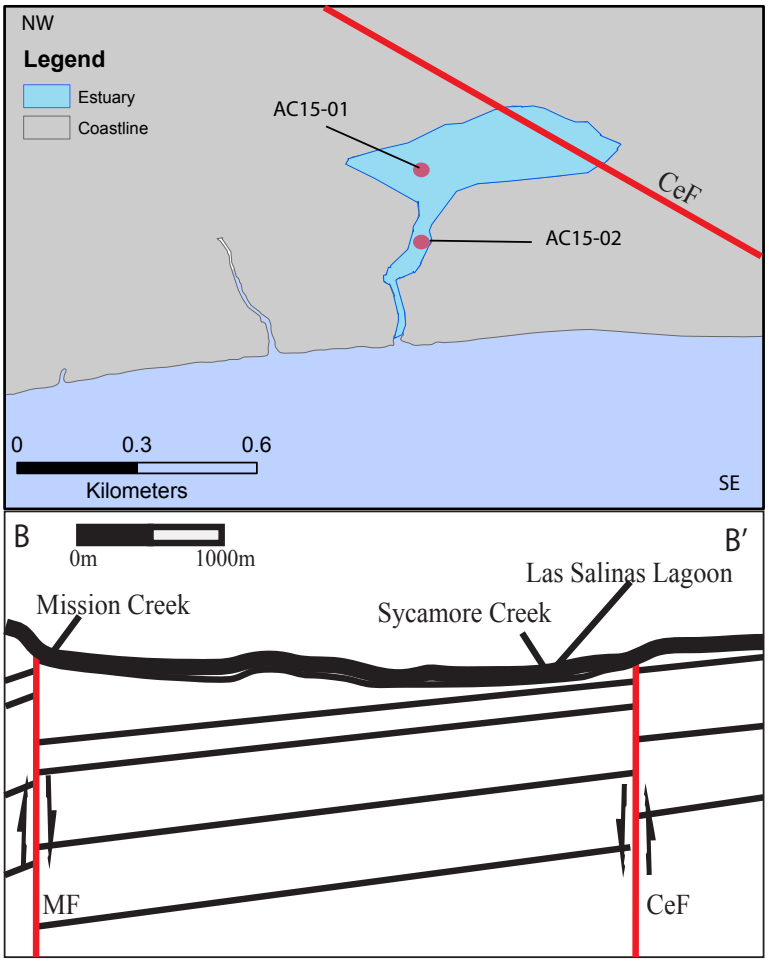

Figure 3: A) Map showing core locations (pink circles) within the Andree Clark Bird Refuge of Las Salinas Lagoon. See Figure 1 for general location. B) Generalized Cross Section based on the surface fault map of B.L. Melosh & E.A. Keller 2013. See Figure 1 for locations of faults. Fault labels are for Mesa Fault (MF) and Santa Barbara Cemetery Fault (CeF). Reference cross section from Figure 1.

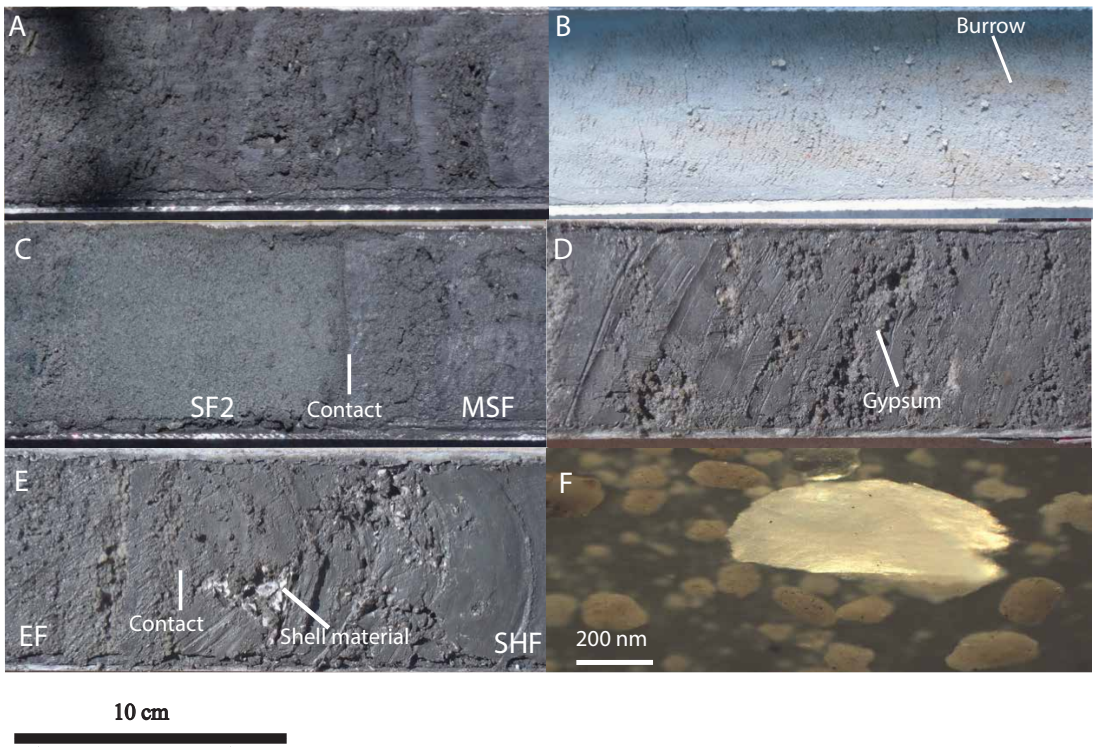

Figure 4: Photographs illustrating the major facies discussed in the text: (A) MSF, (B) SF1, (C) SF2 overlying MFS, (D) EF, (E) SHF underlying facies EF. F) Zoom in of a subsampled section of SHF displaying fecal pellets surrounding a shell fragment

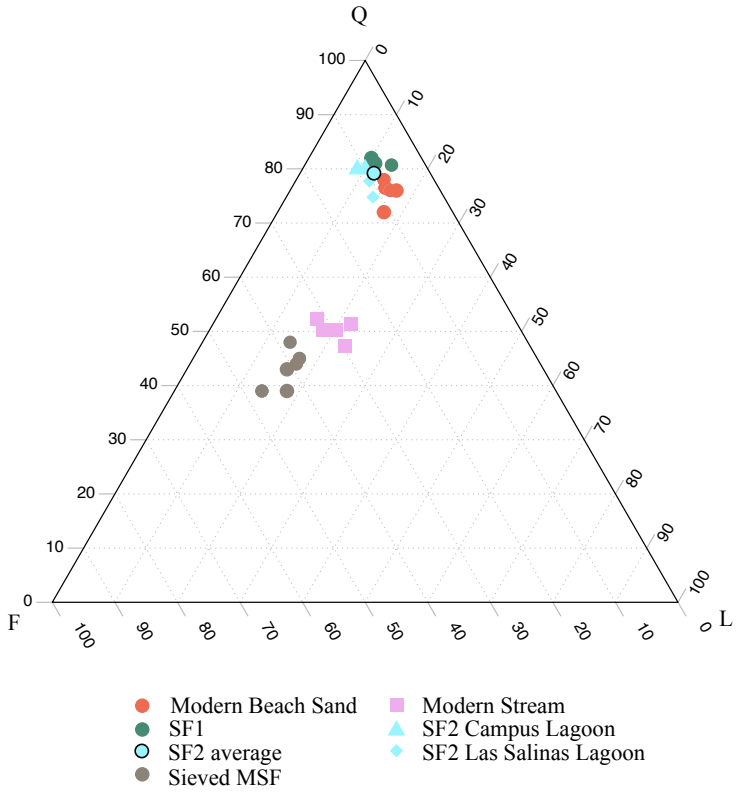

Figure 5: Quartz, Feldspar, Lithic ternary diagram for one modern environment, SF1, SF2, and MSF.

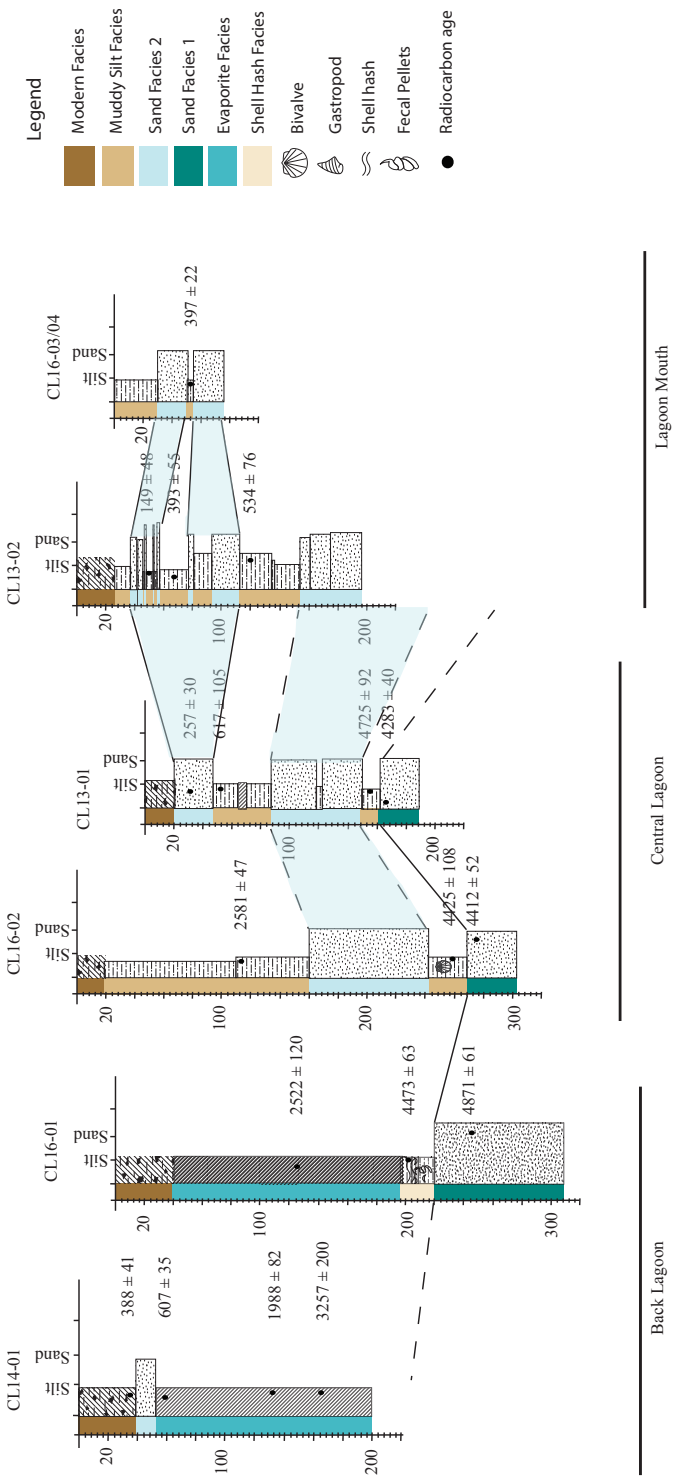
Legend
Modern Facies
Muddy Silt Facies
Sand Facies 2
Sand Facies 1
Evaporite Facies
Shell Hash Facies
Bivalve
Gastropod
Shell hash
Fecal Pellets
Radiocarbon age
CL14-01
CL16-01
CL16-02
CL13-01
CL13-02
CL16-03/04
Silt
Sand
388 ± 41
607 ± 35
1988 ± 82
3257 ± 200
2522 ± 120
4473 ± 63
4871 ± 61
2581 ± 47
4425 ± 108
4412 ± 52
4725 ± 92
4283 ± 40
257 ± 30
617 ± 105
149 ± 48
393 ± 55
534 ± 76
397 ± 22
Back Lagoon
Central Lagoon
Lagoon Mouth

Figure 6: Dip-oriented cross-section of Campus Lagoon hung on a datum relative to water depth to top of core. Opaque polygons denote correlations.

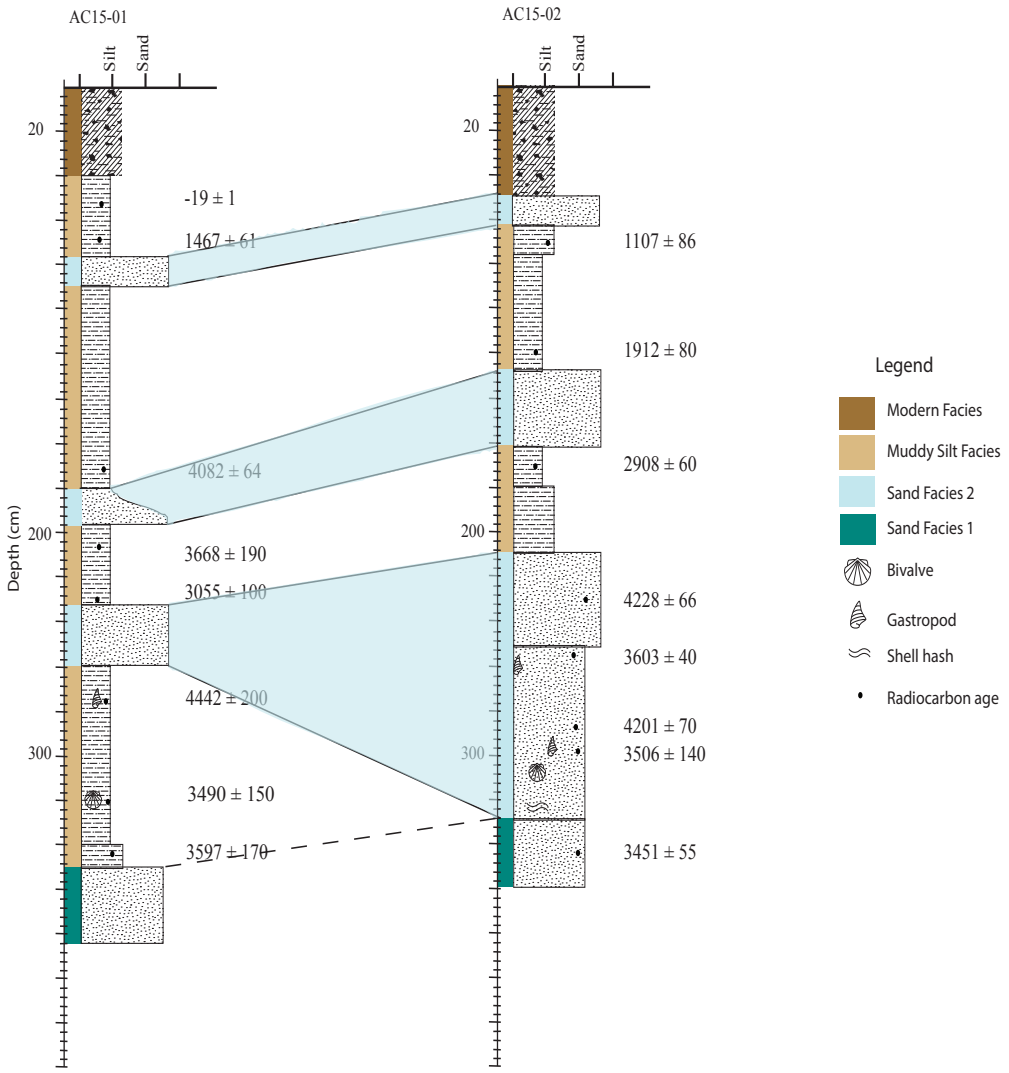

Figure 7: Cores descriptions from Las Salinas lagoon

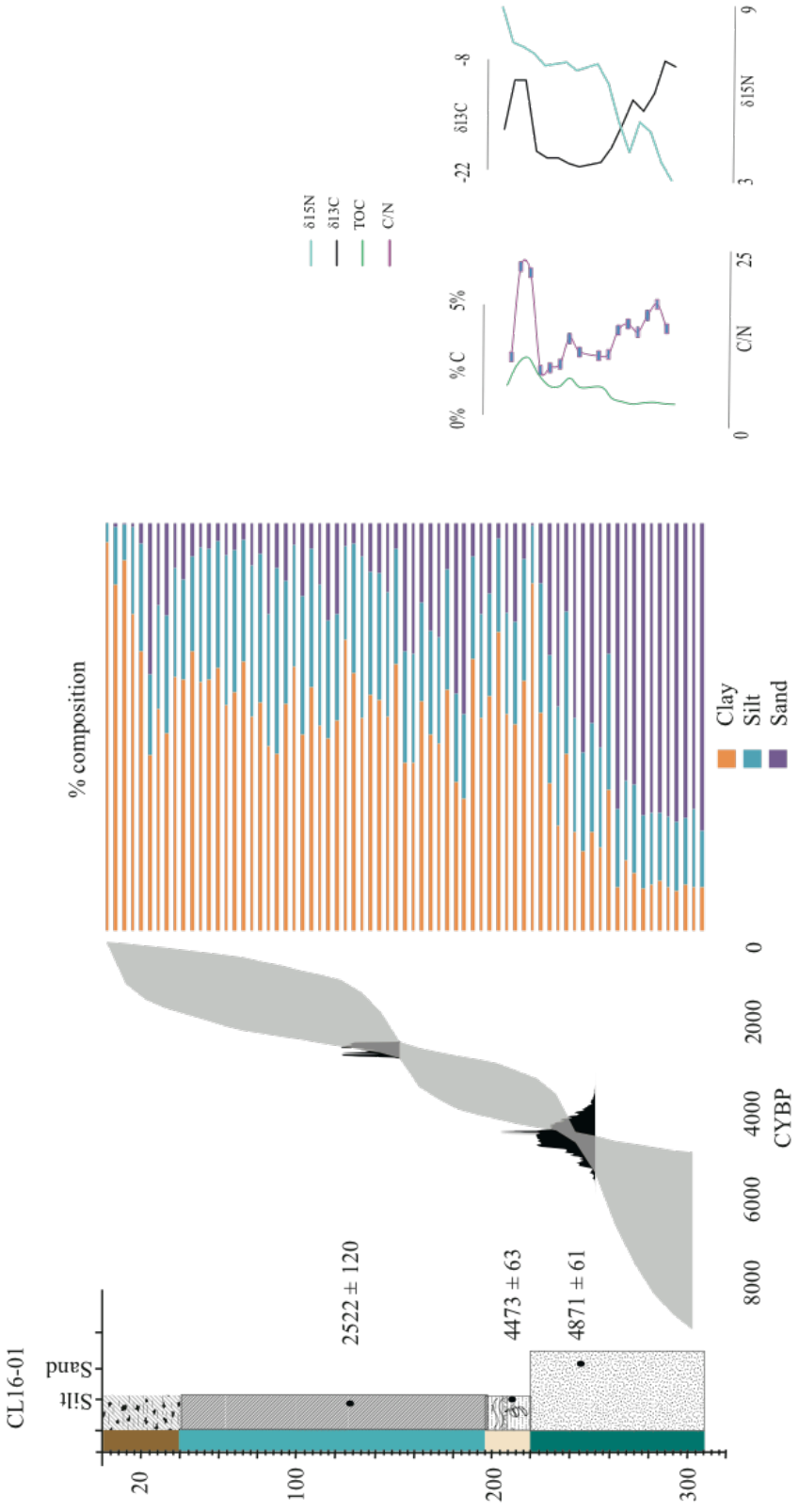

Figure 8: Core lithology of Campus Lagoon (CL16-01) accompanied by an age depth model, grain size data (by %), and isotope data.

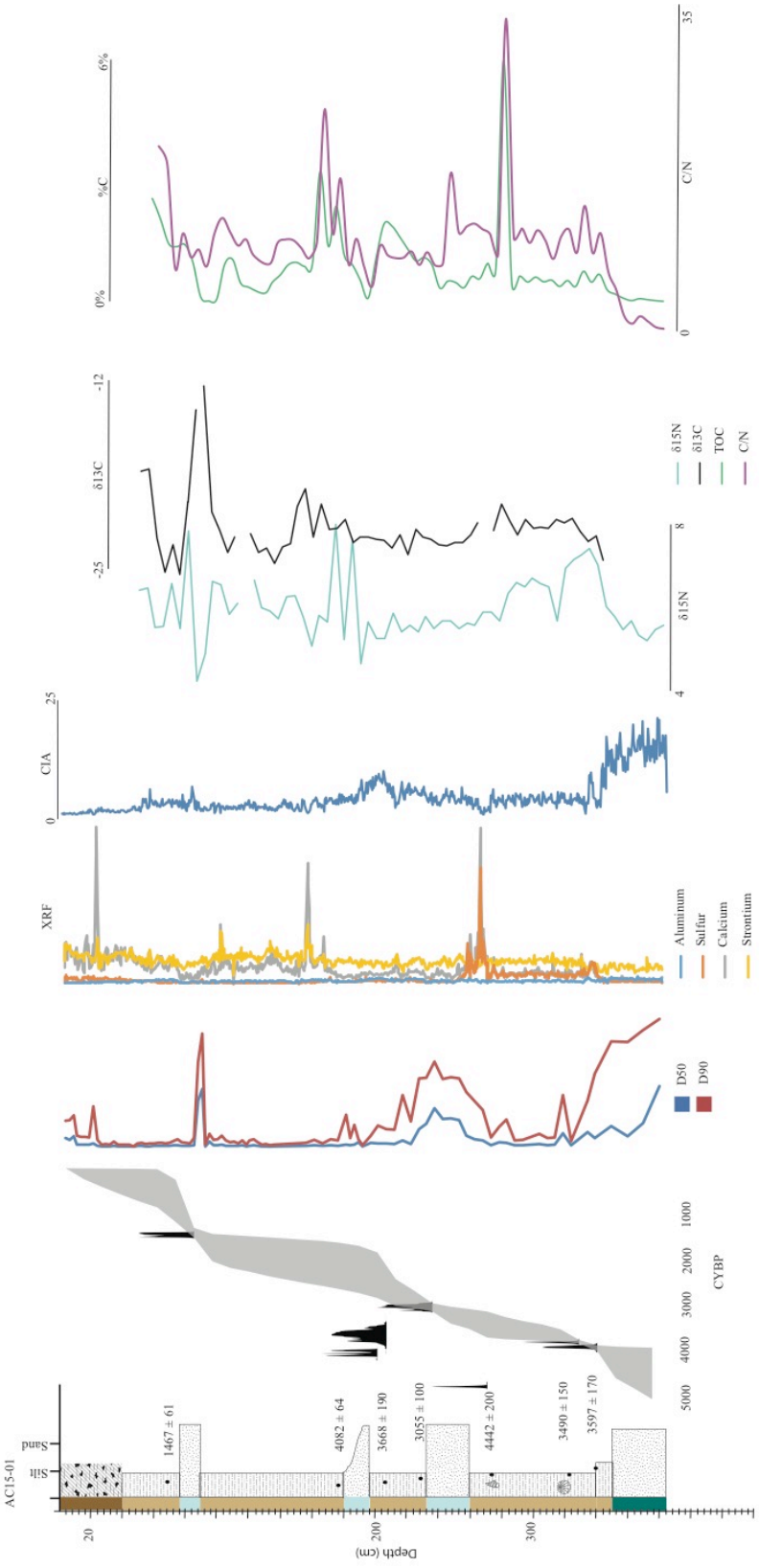
AC15-01
Silt
Sand
1467 ± 61
4082 ± 64
3668 ± 190
3055 ± 100
4442 ± 200
3490 ± 150
3597 ± 170
Depth (cm)
20
200
300
CYBP
5000
4000
3000
2000
1000
D50
D90
XRF
Aluminum
Sulfur
Calcium
Strontium
CIA
0
25
δ15N
δ13C
TOC
C/N
-25
-12
4
8
0%
%C
6%
0
C/N
35

Figure 9: Core log, age depth model, grain size, relative abundance of ions, CIA, $\delta^{13}C_{org}$ (black, per mil), $\delta^{15}N$ (blue, per mil), TOC (purple, wt%), TN (green, wt%) for Las Salinas Lagoon core AC15-01. See Figure 3 for core location.

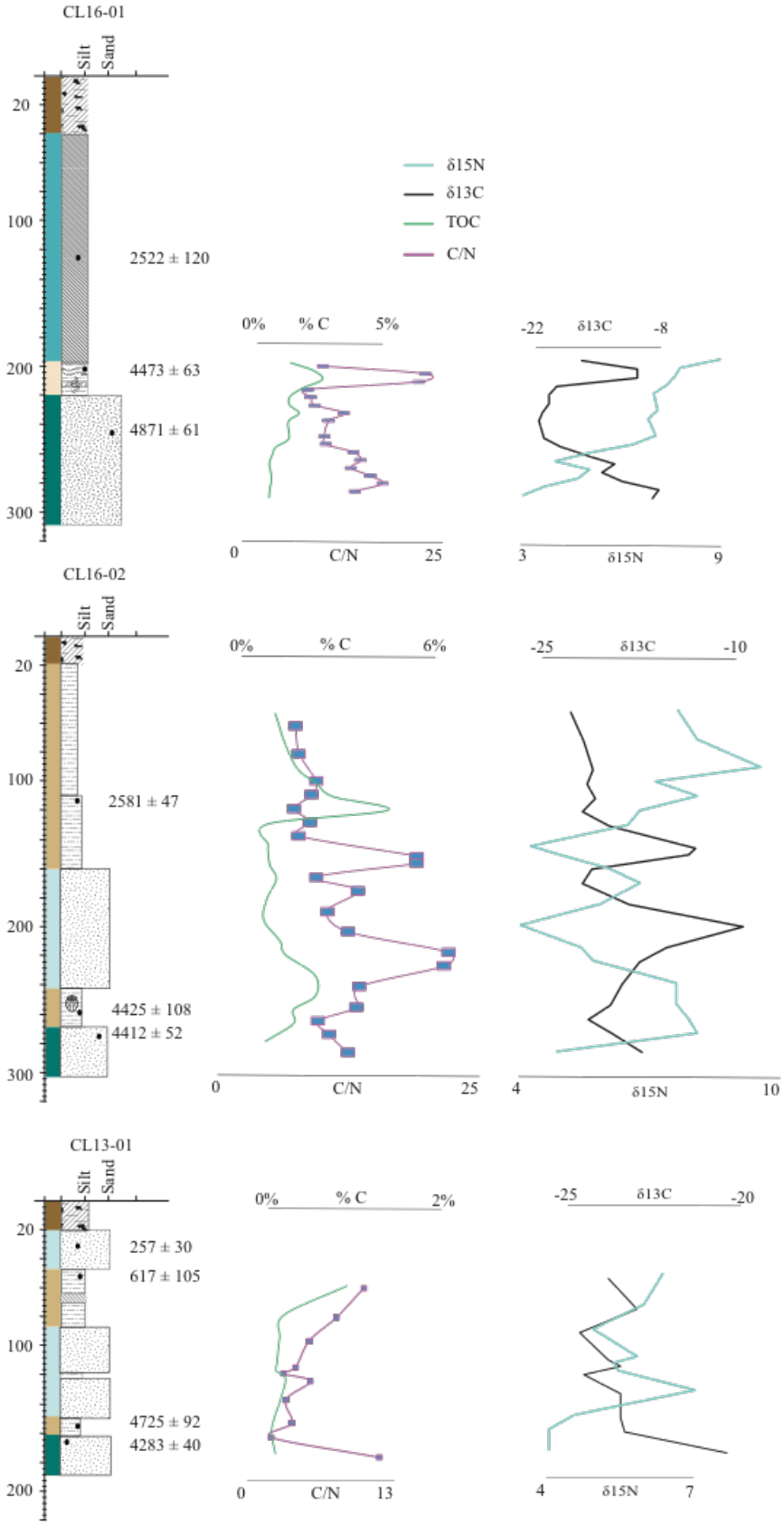
CL16-01
Silt
Sand
20
100
200
300
2522 ± 120
4473 ± 63
4871 ± 61
δ15N
δ13C
TOC
C/N
0%
% C
5%
0
C/N
25
-22
δ13C
-8
3
δ15N
9
CL16-02
Silt
Sand
20
100
200
300
2581 ± 47
4425 ± 108
4412 ± 52
0%
% C
6%
0
C/N
25
-25
δ13C
-10
4
δ15N
10
CL13-01
Silt
Sand
20
100
200
257 ± 30
617 ± 105
4725 ± 92
4283 ± 40
0%
% C
2%
0
C/N
13
-25
δ13C
-20
4
δ15N
7

Figure 10: Core description, %C (Purple), C/N ratio (Green), $\delta^{13}C$ (Black), $\delta^{15}N$ (Blue) for three cores examined from Campus Lagoon. See Figure 2 for core locations.

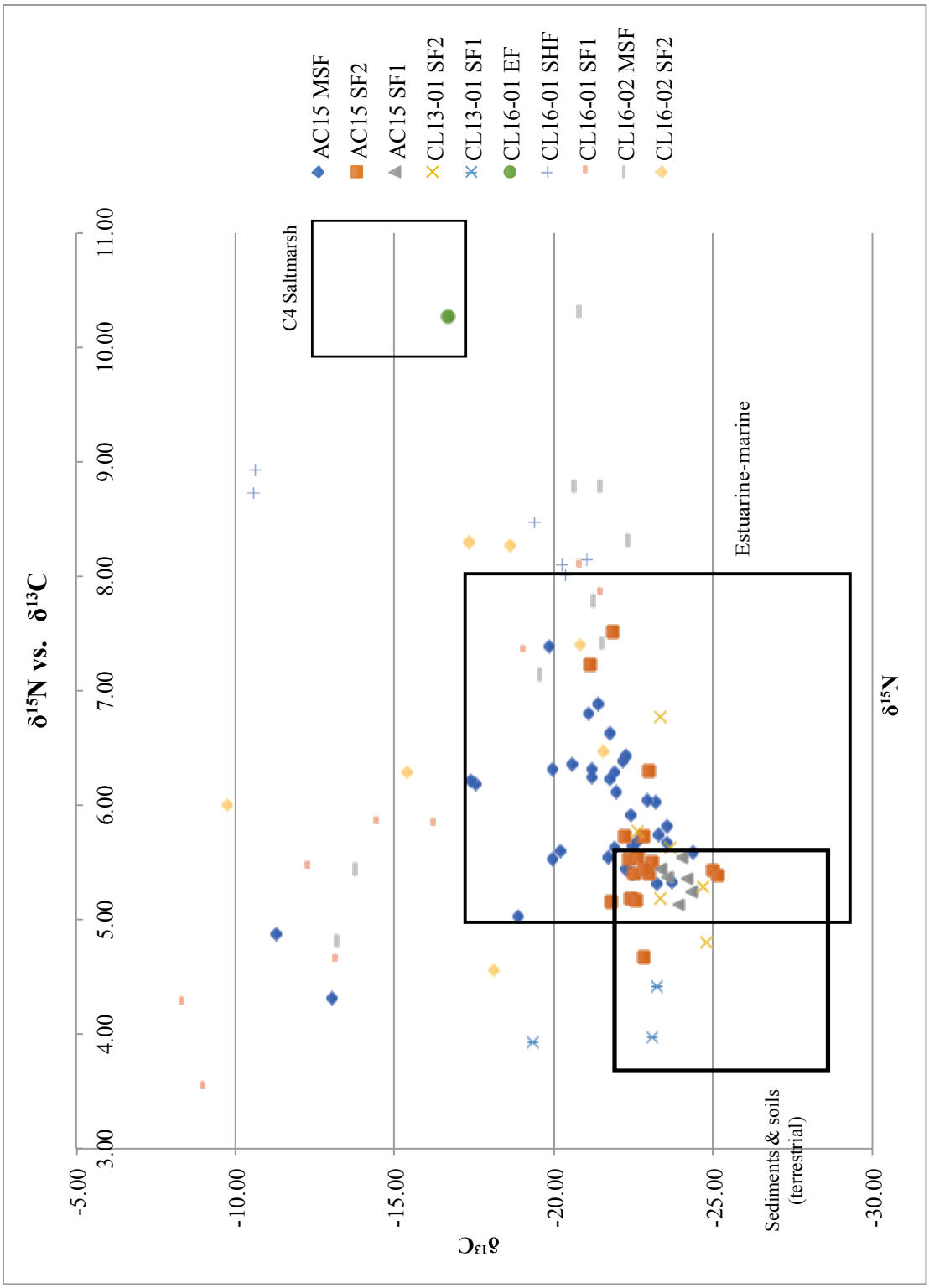

Figure 11: Cross plot of Carbon isotope values vs. Nitrogen isotope values from this study (Red) compared to those used to differentiate environment from (Cloern et al., 2002). Boxes highlight environments determined by (Cloern et al., 2002).

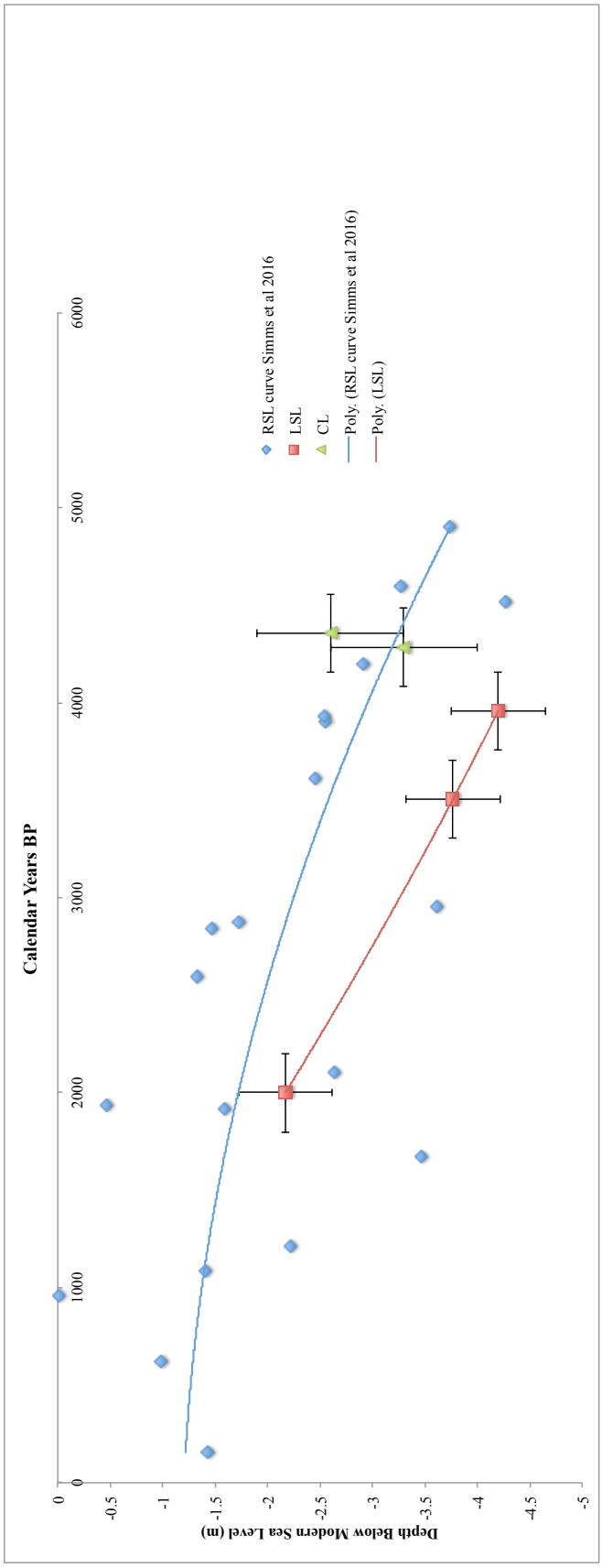
Calendar Years BP
0
1000
2000
3000
4000
5000
6000
Depth Below Modern Sea Level (m)
0
-0.5
-1
-1.5
-2
-2.5
-3
-3.5
-4
-4.5
-5
RSL curve Simms et al 2016
LSL
CL
Poly. (RSL curve Simms et al 2016)
Poly. (LSL)

Figure 12: Graph illustrating elevations of *Cerithidea californica* for Campus Lagoon (CL) and Las Salinas Lagoon (LSL) compared to the relative sea-level curve of (Reynolds and Simms, 2015).

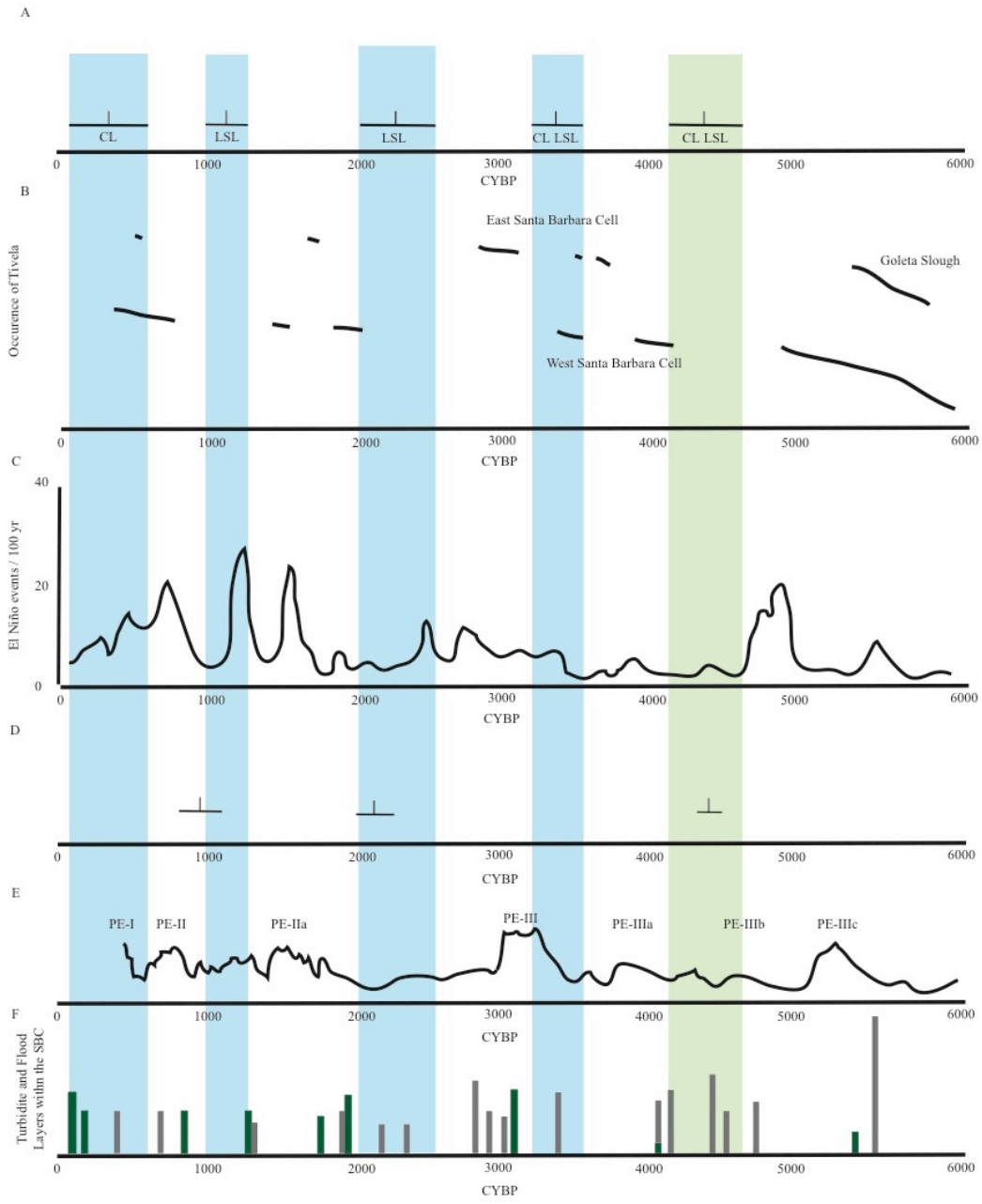

Figure 13: Correlation figure: a) Occurrence of SF2 facies described in this paper. b) Occurrence of Tivela clam species in the Santa Barbara Cell over time (modified from (Masters, 2006)). c) El Niño proxy record from Laguna Pallcacocha (modified from (Moy et al., 2002)). d) Emergence ages for marine terraces identifying earthquake activity along the Pitas Point Fault (Rockwell et

al., 2016). e) Record of pluvial events from Lower Bear Lake, CA (Kirby et al., 2012). f) Record of turbidites (green) and storm flood deposits (grey) from the Santa Barbara Channel (Du et al., 2018). Blue Bars note correspondence between beds of SF2, Beach reduction, El Niño frequency, earthquake events, pluvial episodes from Lower Bear Lake, and storm deposits/turbidites from the Santa Barbara Channel.

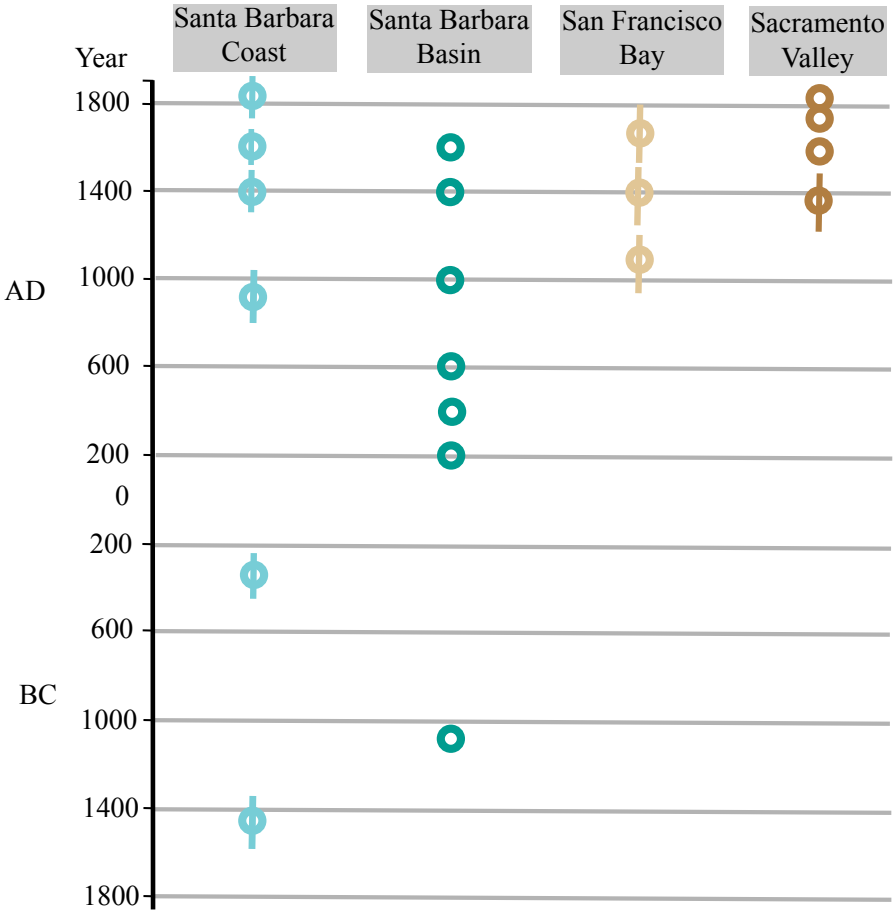

Figure 14: Ages of SF2 deposits from this study (Blue) plotted throughout time accompanied by ages of hypothesized storm deposits from the Santa Barbara Basin (Green) (Du et al., 2018), sediment cores from a San Francisco Bay marsh (Beige) (Malamud-Roam and Lynn Ingram, 2004), and lacustrine sediment cores in the Sacramento Valley (Brown) (Sullivan et al., 2015).

Number	lab code	Core ID	Depth interval	14C age (BP)	Error	CY BP (1950)	2 sigma range (years)	material
1	186409	AC15-01	55	1.56 MF	0.002	-19	1	Charcoal
2	186410	AC15-01	70	1580	20	1467	61	Charcoal
3	200620	AC15-01	102	10380	350	*	*	Charcoal
4	200621	AC15-01	180	3730	25	4082	64	Charcoal
5	186411	AC15-01	205	3410	80	3668	190	Charcoal
6	200622	AC15-01	230	2915	25	3055	100	Charcoal
7	200623	AC15-01	275	4585	25	4442	200	Carbonate
8	186288	AC15-01	330	3865	15	3490	150	Carbonate
9	200650	AC15-01	340	3955	20	3597	170	Carbonate
10	183701	AC15-02	70	1170	15	1107	86	Charcoal
11	186416	AC15-02	120	1960	40	1912	80	Charcoal
12	183704	AC15-02	173	2805	25	2908	60	Charcoal
13	183704	AC15-02	233	3835	15	4228	66	Charcoal
14	183705	AC15-02	255	3360	15	3603	40	Charcoal
15	183686	AC15-02	287	3820	20	4201	70	Charcoal
16	183687	AC15-02	300	3880	15	3506	140	Carbonate
17	183698	AC15-02	344	3830	15	3451	55	Carbonate
18	200624	CL13-01	50	145	30	149	48	Charcoal
19	200625	CL13-01	67	305	20	393	55	Charcoal
20	200626	CL13-01	115	520	25	534	76	Charcoal
21	5757	CL13-02	42	252	15	257	30	Charcoal
22	186414	CL13-02	60	650	90	617	105	Charcoal
23	200627	CL13-02	92	>54000		*	*	Charcoal
24	200629	CL13-02	150	4530	25	4745	92	Charcoal
25	200630	CL16-02	160	6620	35	*	*	Charcoal
26	5756	CL13-02	178	3860	15	4283	40	Charcoal
27	191118	CL14-01	14	690	30	659	31	Charcoal
28	191112	CL14-01	35	305	30	388	41	Charcoal
29	200632	CL14-01	50	580	20	607	35	Charcoal
30	191115	CL14-01	75	11260	70	*	*	Charcoal
31	191116	CL14-01	130	2035	30	1988	82	Charcoal
32	191117	CL14-01	160	3060	80	3257	200	Charcoal
33	183702	CL16-01	115	7930	260	*	*	Charcoal
34	200631	CL16-01	150	2445	45	2522	120	Charcoal
35	183700	CL16-01	238	4030	15	4473	63	Charcoal
36	191111	CL16-01	250	4080	250	4871	61	Charcoal
37	183697	CL16-02	110	2510	15	2581	47	Charcoal
38	200651	CL16-02	250	4470	25	4286	200	Carbonate
39	183690	CL16-02	285	4475	15	4293	120	Carbonate
40	183688	CL16-03	38	1.21 MF	0.002	-34	3	Charcoal
41	183689	CL16-03	45	850	15	756	30	Charcoal
42	183716	CL16-04	42	305	15	397	22	Charcoal

Table 1: Raw and calibrated age data for cores presented and analyzed in this paper. The marine reservoir of 217 years, detailed in the methods section of this work, was used for all carbonate samples. Samples denoted with a * in any column were excluded from analysis due to large analysis error.

Facies	Location	Core (s)	Depth (cm)	Age brackets CYBP	Bchron Age
SF2	Campus Lagoon	CL13-01 , CL13-03/04	35 - 55, 35 - 55	149 (48) - 393 (22)	*
SF2	Campus Lagoon	CL14-01, CL13-02, CL13-01 , CL13-03/04	38 - 50, 20 - 50, 80 - 110, 58 - 75	393 (22) - 617 (105)	*
SF2	Las Salinas Lagoon	AC15-01, AC15-02	78 - 90, 50 - 63	modern -1107 (86)	1050 (200)
SF2	Las Salinas Lagoon	AC15-01, AC15-02	180 - 200, 130 - 165	1912 (80) - 2908 (60)	2250 (300)
SF2	CL & LSL	CL16-02, CL13-02, AC15-01, AC15-02	160 - 240, 90 - 150, 230 - 260, 210 - 320	2581 (47) - 4425 (108)	3400 (150)
SF1	CL & LSL	AC15-01, AC15-02, CL13-02, CL16-02, CL16-01	350, ~320, 160, 270, 220	4425 (88)	4400 (250)

Table 2: List to assist with the chronology section of this manuscript. Beds of described facies are listed by location and as well as their position in cores. Age Brackets and Bchron age depth model ages are given for each bed. * in the bchron column denotes multiple beds of SF2 within the age bracket.

location	core	depth in core	observed RSL	error RSL	age CYBP	error	source
LSL	AC15-01	3.4	0.8	0.45	3957	170	This Study
LSL	AC15-02	1.37	0.8	0.45	2000	200	This Study
LSL	AC15-02	2.97	0.8	0.45	3506	140	This Study
CL	CL13-02	1.8	0.8	0.7	4358	200	Simms et al 2016
CL	CL16-02	2.5	0.8	0.7	4286	200	This Study

location	core	actual depth	predicted paleo Sea Level	subsidence	subsidence rate (mm)	Estuary Average	error
LSL	AC15-01	4.2	2.75	1.45	0.33	0.27	0.75
LSL	AC15-02	2.17	1.75	0.42	0.21		
LSL	AC15-02	3.77	2.65	1.12	0.27		
CL	CL13-02	2.6	3.2	-0.5	-0.1	0	0.9
CL	CL16-02	3.3	3.2	0.1	0.1		

Table 3: Ages of *Cerithidea californica* and calculated subsidence rates.
* Denotes ages derived from Bchron age depth models.

Supporting Figures:

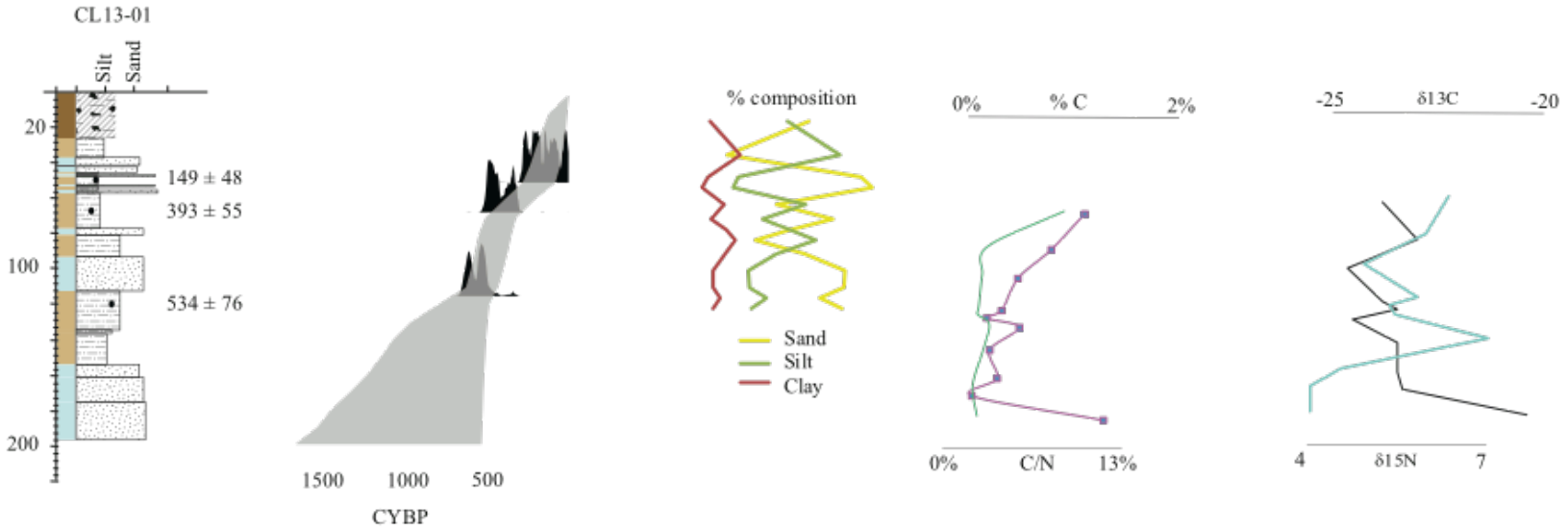
CL13-01
Silt
Sand
20
100
200
149 ± 48
393 ± 55
534 ± 76
1500
1000
500
CYBP
% composition
Sand
Silt
Clay
0%
% C
2%
0%
C/N
13%
-25
δ13C
-20
4
δ15N
7

Supporting Figure 1: Core lithology of Campus Lagoon (CL13-01) accompanied by an age depth model, grain size data (by %), and isotope data.

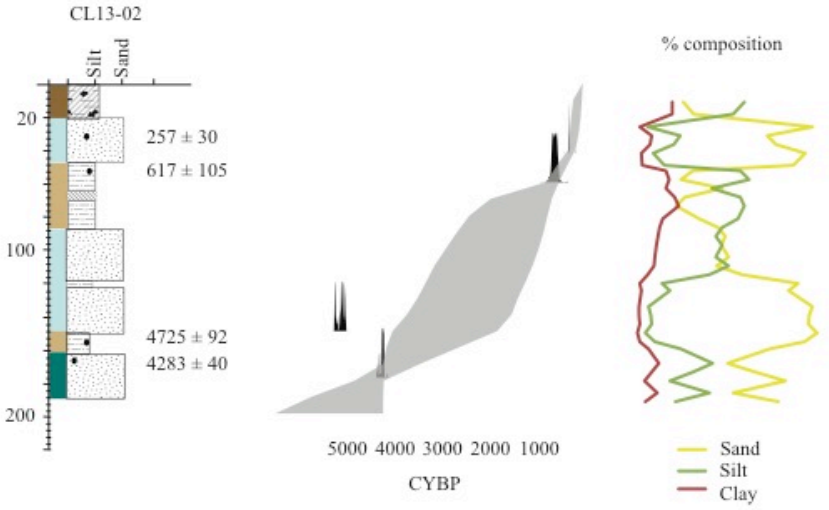

Supporting Figure 2: Core lithology of Campus Lagoon (CL13-02) accompanied by an age depth model and grain size data (by %).

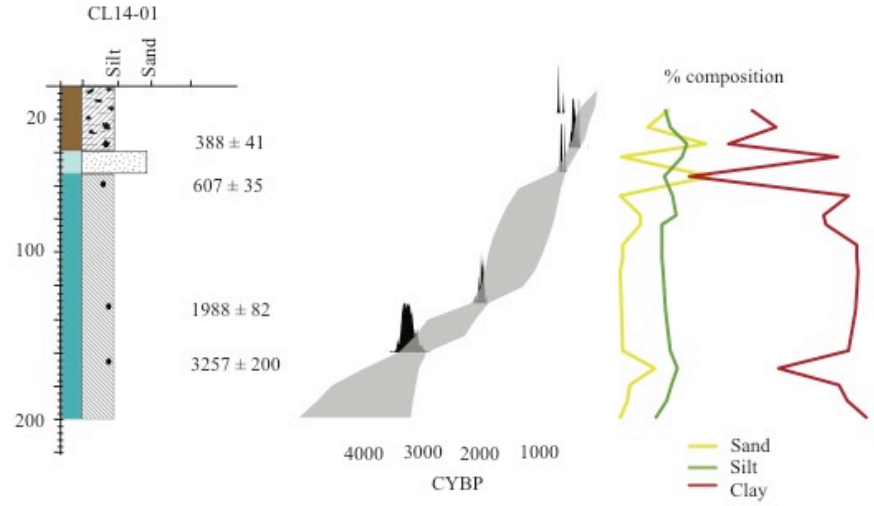

Supporting Figure 3: Core lithology of Campus Lagoon (CL14-01) accompanied by an age depth model and grain size data (by %).

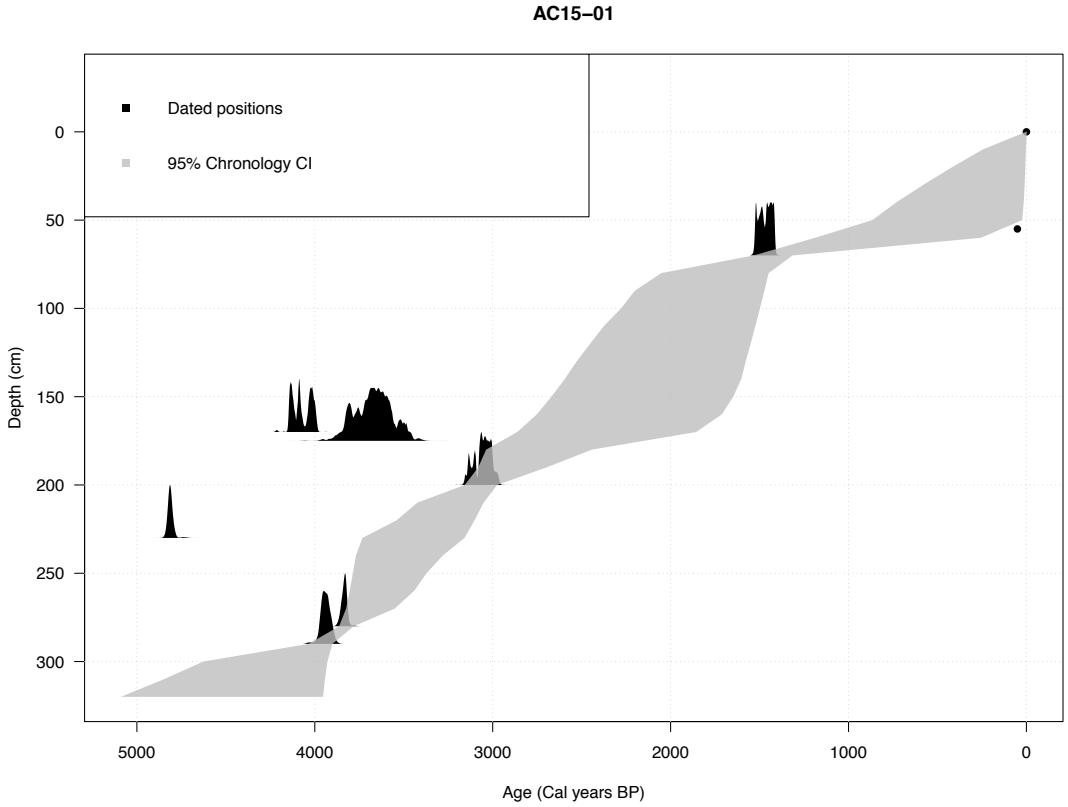
AC15–01
Dated positions
95% Chronology CI
Depth (cm)
0
50
100
150
200
250
300
5000
4000
3000
2000
1000
0
Age (Cal years BP)

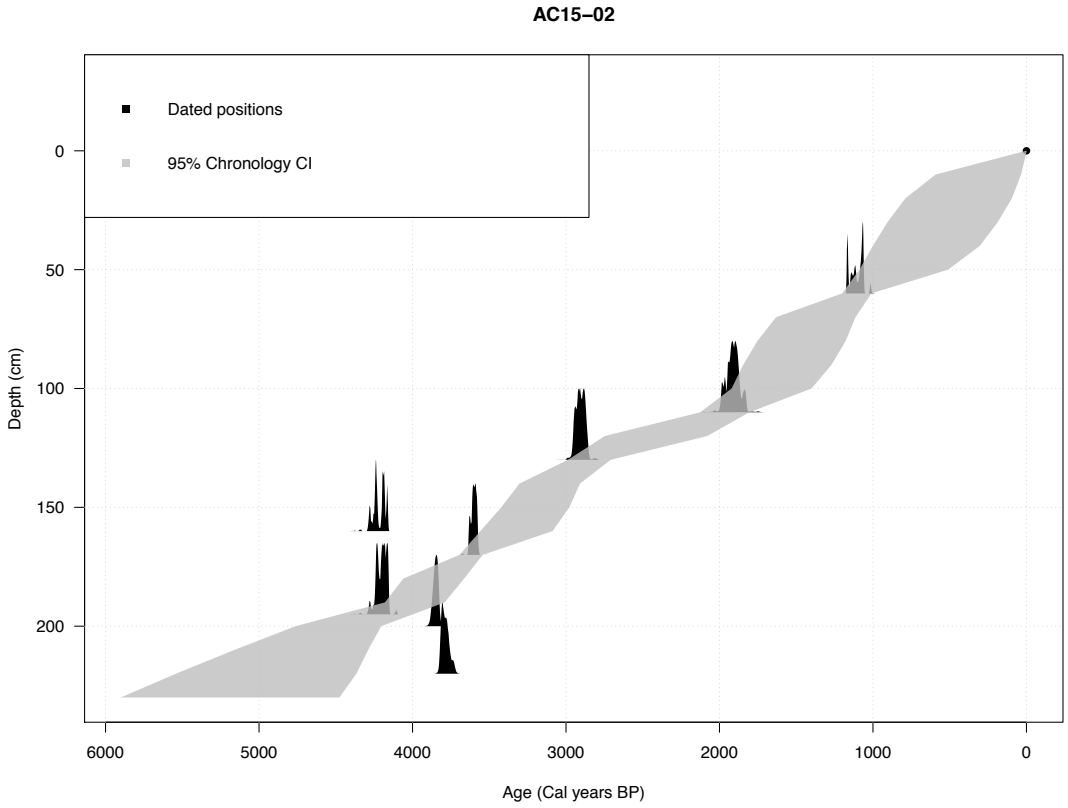

Supporting Figure 4: Bchron age depth models for cores from Las Salinas Lagoon. Due to the determination of sediment accumulation as non-linear (beds of SF2 deposited instantaneously), those beds were "subtracted" from the core depth to better assign single ages to their occurrence as applied in (Wright et al., 2017)

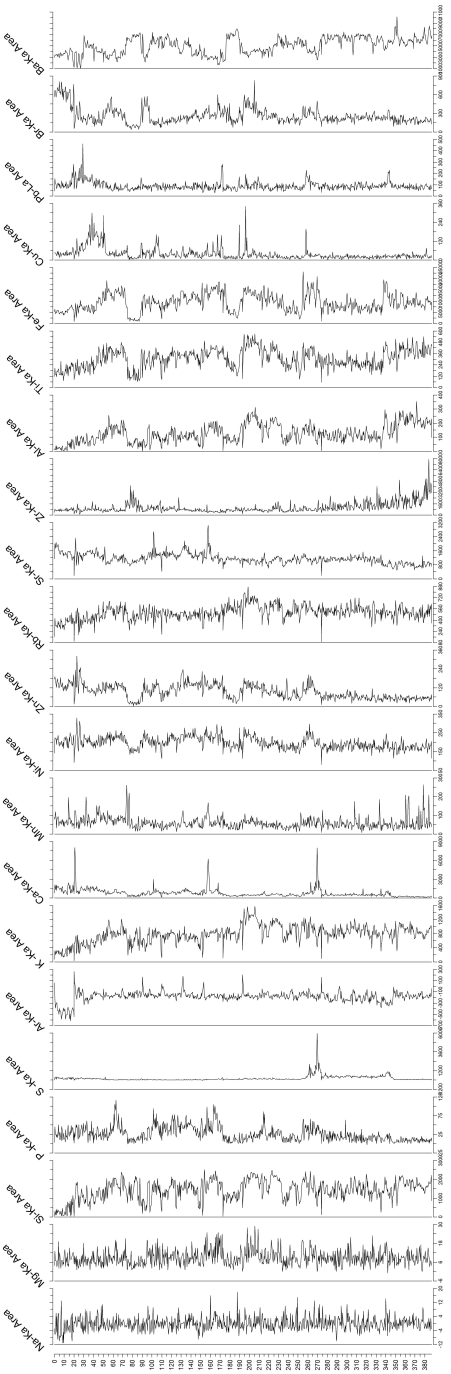

Supporting Figure 5: Raw XRF measurements from core scans of AC15-01. (Ejarque, A. Personal Communication.)

Supporting Figure 6: 1852 T-sheet of the Santa Barbara coastline detailing paleo-creek locations relative to Las Salinas Lagoon pre-modification. (San Francisco Estuary Institute)

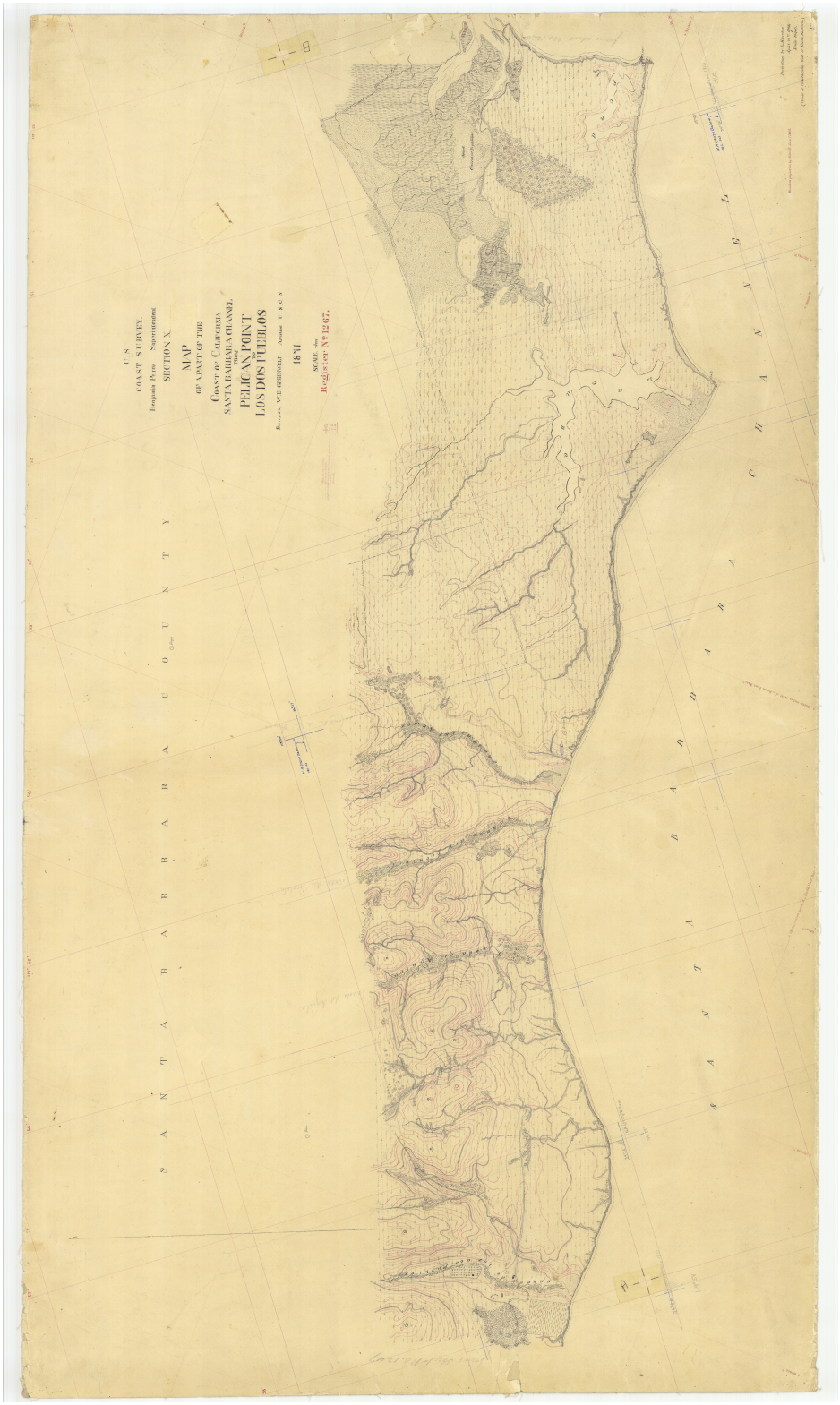

Supporting Figure 7: 1870 T-sheet of the Santa Barbara Basin coastline West of Pelican Point (Campus Point), detailing beach and marine terrace features relative to Campus Lagoon pre-development and modification. (San Francisco Estuary Institute)